A spectral approach for damage quantification in stochastic dynamic systems

M.R. Machado[a,*], S. Adhikari[b], J.M.C. Dos Santos[a]

[a] *University of Campinas, UNICAMP-FEM-DMC, Rua Mendeleyev, 200, CEP 13083-970, Campinas, SP, Brazil.*
[b] *Swansea University, Singleton Park, Swansea SA2 8PP, UK.*

Abstract

Intrinsic to all real structures, parameter uncertainty can be found in material properties and geometries. Many structural parameters, such as, elastic modulus, Poisson's rate, thickness, density, etc., are spatially distributed by nature. The Karhunen-Loève expansion is a method used to model the random field expanded in a spectral decomposition. Once many structural parameters can not be modelled as a Gaussian distribution the memoryless nonlinear transformation is used to translate a Gaussian random field in a non-Gaussian. Thus, stochastic methods have been used to include these uncertainties in the structural model. The Spectral Element Method (SEM) is used to model the structure. It is also developed to express parameters as spatially correlated random field in his formulation. In this paper, the problem of structural damage detection under the presence of spatially distributed random parameter is addressed. An explicit equation to assess damage is proposed based on the mathematical SEM formulation. Numerical examples in an axially vibrating undamaged and damaged structure with distributed parameters are analysed.

Keywords: Damage detection, Uncertainties quantification, Random field, Inverse problem.

*Corresponding author. Tel.: +55 11987957555
Email address: mrmomarcela@gmail.com (M.R. Machado)

1. Introduction

In general, changes in either global or local structural properties can be associated with damage parameters. Over the last decades, many works have been performed to develop vibration-based non-destructive evaluation (NDE) methods, which allow a damage to be localised and quantified from modal parameters and dynamic response [1, 2]. However, these techniques are well suited to detect large damages rather than small damages like a crack. Structural crack does not impose appreciable changes at low-frequency and the global structural behaviour is unaffected. The presence of a crack in a structure introduces a local flexibility that affects its vibration response. It also generates changes in the elastic waves that propagate in the structure. New and recent researches about damage quantification are concentrated on methods that use elastic wave propagation in structures at medium and high frequencies [3, 4, 5, 6, 7]. They use the inherent material property that discontinuities, such as a crack, generate changes in the elastic waves propagating in the structure. There are some particular advantages of elastic wave-based damage quantification, such as their capacity to propagate over significant distances and high sensitivity to discontinuities near the wave propagation path.

The spectral element method (SEM) [8, 9] is based on the analytical solution of the displacement wave equation, written in the frequency domain. The element is tailored with the matrix ideas of the finite element method (FEM), where the interpolation function is the exact solution of wave equation. This approach can be called by different names, such as the dynamic stiffness method [10, 11, 12, 13, 14, 15, 16, 17, 18, 19, 20], spectral finite element method [21, 22] and dynamic finite element method [23, 24]. Built-up structures with geometrically uniform members can be modelled by a single spectral element. This can reduce significantly the total number of degrees of freedom compared to other similar methods. Since the method is based on the wave equation it performs well at medium and high-frequency bands. However, there are still some drawbacks, such as difficulties to model non-uniform members and to apply arbitrary

boundary conditions for 2D and 3D elements. To work with the SEM in time domain is needed to apply the Fast Fourier Transform (FFT), it is largely used for damage detection studies. Although, in time domain responses is observed the signal wrap-around behaviour as a consequence of using the discrete inverse Fourier Transform. To avoid the wrap-around behaviour a useful element is considered, the throw-off element. For more details about the throw-off element and wraparound effects see in Ref. [25, 3, 26]. The treatment of uncertainties using spectral element method is recent [27, 28], and very few was made related to detection and assessment of the damage. Recently, researchers have presented works in damage detection using wave propagation in the context of uncertainty quantification and stochastic SEM model [29, 30, 31, 32].

Structural health monitoring (SHM) can be defined as a process that involves the observation of a structure over time using periodically spaced measurements [33, 34]. Based on this measurement the current state of the undamaged system can be determined. The inverse problem approach is a technique where the structural model parameters can be identified (or the damage can be detected) based on the frequency response data [35]. In general, the structural damage is a local phenomenon and produces a stiffness reduction, which changes the frequency response of the system [36]. Damage estimation is based on the optimisation methods [37, 38], which can be used to solve the inverse problem. These techniques consist in minimising the differences between the numerical model and experimental test responses by using a parameter estimation procedure [39, 40, 41]. In structural dynamic testing, it is common practice to measure the data in the form of frequency response functions (FRF). The knowledge about a particular structure is contained in a theoretical model and can be constructed using a numerical method. Many papers written on this subject have been used with FEM [42] and the experimental modal analysis (EMA) [43]. In order to include parameter variability to damage detection and parameter estimation methods, recent researchers started with the stochastic approaches. Some authors [44, 30, 29] have proposed stochastic methods to characterise and identify the damage including random parameters based on probabilistic

approaches. Arda Vanli and Sungmoon Jung [45], and Khodaparast and Mottershead [46] present a probabilistic and stochastic model updating method to improve damage location and damage quantification prediction of a structural health monitoring system.

Damage quantification methods assume that they can provide a numerical dynamic response very close to that of a real structure. Parameters, modelling, and measurement uncertainties are inherently involved in the damage quantification procedure. The stochastic approach in the framework to understand the magnitude of uncertainty for simulation results is approached. It can be treated in the scope of the random variable, which is understood as a function defined on a sample space whose outputs are numerical values, and random field corresponds to naturally spatially varying properties [47]. The reference and most widely used method is the Monte Carlo (MC) simulation. It is a sampling method which can generate independent random variables, based on their probability distributions, and solving the deterministic problem for each realisation. By collecting an ensemble of solutions the statistical moments can be calculated [48]. Although easy to apply a large number of samples are needed to obtain convergence, which means high computational costs. The Direct method consists in directly applying the statistical moment equations to obtain the random solutions. The unknowns are the moments and their equations are derived by taking averages over the original stochastic governing equations. The problem is that a statistical moment almost always requires information about higher moments. A non-sampling approach, known as Perturbation method, consists of expanding the random fields in a truncated Taylor series around their mean. Its main drawback is the limitation of the magnitude of uncertainties which cannot be too large, typically less than 10% [49]. Another method widely used as considering random field is the Karhunen-Loève (KL) expansion [50, 49]. The KL expansion may be used to discretize the random field by representing it by scalar independent random variables and continuous deterministic functions. By truncating the expansion the number of random variables becomes finite and numerically treatable. Several authors use the KL expansion to model Gaus-

sian random processes, however it is possible to extend the KL expansion to non-Gaussian processes [51, 52, 53, 54, 55, 56, 57, 58].

This work uses a rod structure modelled by SEM to assess a damage with parameter uncertainty related to material property and geometry. A rod structure was used to avoid the effects of evanescent waves at the first moment. The cross section area and Young's modulus were considered as a non-Gaussian random variable and as non-Gaussian distributed random field expanded by KL. A non-Gaussian process is expressed as a memoryless transformation of an underlying Gaussian process. The proposed stochastic damage quantification technique combines SEM with the stochastic approaches and Structural Health Monitoring procedure. Based on the mathematical structure model and the relation between undamaged and damaged structure an explicit formulation to estimate the damage depth was developed. This technique allows quantifying the damage by using direct structure's dynamic response and to improve the control over the numerical model dispersion when it is under a stochastic environment. One of the main advantage of the proposed spectral approach is that the analytical formulations are frequency independent. Therefore, unlike conventional finite element based approaches, there is no theoretical limitation on higher frequency ranges.

2. Spectral element method for stochastic systems

The spectral element method is similar to FEM with the exception of two important aspects. SEM is frequency domain formulation and the spectral element form function is the exact solution of wave equation. Based on this latter aspect the number of elements required for a spectral model will coincide with the number of discontinuities in the structure. In this section, it will be presented the stochastic formulation for undamaged and damaged rod spectral element. A damage quantification technique considering the stochastic process is presented. The new contribution consists in to obtain the structural response and crack parameters variability based on the uncertainty of structural parameter

spatially distributed, using the random variable and random field approaches. The random field is expressed based on Karhunen-Loève expansion. A nonlinear memoryless transformation is used to express a non-Gaussian random field by means of a Gaussian random field.

2.1. Undamaged rod

Deterministic

In this section, the fundamental equations are derived for a longitudinal wave propagation in an undamaged rod, a more extensive formulation can be found in [8, 9]. The elementary rod theory considers this structure as long, slender, and assumes that it supports only 1-D axial stress. Figure 1 shows an elastic two nodes rod element with one degree-of-freedom per node, uniform rectangular cross-section subjected to dynamic forces.

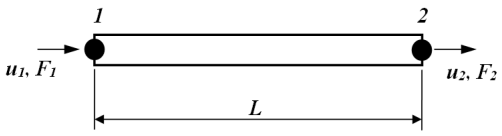

Figure 1: Two nodes undamaged rod spectral element.

The undamped equilibrium equation with deterministic parameters at frequency domain can be written as [8]:

$$EA_0 \frac{d^2u(x)}{dx^2} + \omega^2 \rho A_0 u(x) = q(x), \tag{1}$$

where A is the cross-section area, ρ is the volume mass density, EA is the longitudinal rigidity, ρA is the mass per unit of length, u is the longitudinal displacement, q is the distributed external force, and ω is the circular frequency. The subscript 0 indicates the mean values. A hysteretic structural damping is assumed and introduced into the model formulation by adding the damping factor in the Young's modulus, in a deterministic case $E_0 = E_0 + E_0 i\eta$, where η is damping factor and $i = \sqrt{-1}$ [8]. In a stochastic case $E(\theta) = E(\theta) + E_0 i\eta$,

where the random part of the Young's modulus is real positive defined and the structural damping factor multiply the Young's modulus mean value. The subscripts 1 and 2 denote values at the element rod node numbers 1 and 2, respectively. The homogeneous solution of eq. (1) is given by,

$$u(x) = a_1 e^{-ikx} + a_2 e^{-ik(L-x)} = \mathbf{s}(x,\omega)\mathbf{a}, \tag{2}$$

where L is the rod element length, $k = \omega/c$ is the wavenumber corresponding to the propagating wave in one direction, and $c = \sqrt{\rho A/EA}$ is the phase speed. In this case, the propagation is assumed to be non-dispersive as all frequency components travel at the same speed, so that the shape of the travelling wave remains the same, and

$$\mathbf{s}(x,\omega) = \{e^{-ikx}\ e^{-ik(L-x)}\}, \qquad \mathbf{a} = \left\{ \begin{array}{c} a_1 \\ a_2 \end{array} \right\} \tag{3}$$

The spectral nodal displacements of the rod can be related with the displacement field as,

$$\mathbf{d} = \left\{ \begin{array}{c} u_1 \\ u_2 \end{array} \right\} = \left\{ \begin{array}{c} u(0) \\ u(L) \end{array} \right\} \tag{4}$$

By substituting eq. (2) into the right side of eq. (4) it has

$$\mathbf{d} = \left[\begin{array}{c} \mathbf{s}(0,\omega) \\ \mathbf{s}(L,\omega) \end{array} \right] \mathbf{a} = \mathbf{G}(\omega)\mathbf{a} \tag{5}$$

where

$$\mathbf{G}(\omega) = \left[\begin{array}{cc} 1 & e^{-ikL} \\ e^{-ikL} & 1 \end{array} \right] \tag{6}$$

The frequency-dependent displacement within an element is interpolated from the nodal displacement vector $\mathbf{d}$, by eliminating the constant vector $\mathbf{a}$ from eq. (2) by using eq. (5) it has

$$u(x,\omega) = \mathbf{g}(x,\omega)\mathbf{d}, \tag{7}$$

where the shape functions are given by,

$$\mathbf{g}(x,\omega) = \mathbf{s}(x,\omega)\mathbf{G}^{-1}(\omega) = \{g_1\ g_2\} \tag{8}$$

with $g_1 = \csc(kL)\sin[k(L-x)]$ and $g_2 = \csc(kL)\sin(kx)$. A generalized longitudinal displacement at any arbitrary point in the rod element is given by $u(x) = g_1(x)u_1 + g_2(x)u_2$, and $\mathbf{\Gamma}(\omega) = \mathbf{G}^{-1}(\omega)$. Mass and stiffness matrices are obtained as:

$$\mathbf{K}_0(\omega) = EA_0\ \mathbf{\Gamma}^T(\omega)\left[\int_0^L \mathbf{s}'^T(x,\omega)\mathbf{s}'(x,\omega)dx\right]\mathbf{\Gamma}(\omega), \tag{9}$$

$$= \frac{EA_0k}{2}\begin{bmatrix} \csc^2(kL)(2kL+\sin(2kL))/2 & -(kL\cot(kL)+1)\csc(kL) \\ -(kL\cot(kL)+1)\csc(kL) & \csc^2(kL)(2kL+\sin(2kL))/2 \end{bmatrix}.$$

$$\mathbf{M}_0(\omega) = \rho A_0\ \mathbf{\Gamma}^T(\omega)\left[\int_0^L \mathbf{s}^T(x,\omega)\mathbf{s}(x,\omega)dx\right]\mathbf{\Gamma}(\omega), \tag{10}$$

$$= \frac{\rho A_0}{2k}\begin{bmatrix} \big(\cot(kL) - kL\csc^2(kL)\big) & (kL\cot(kL)-1)\csc(kL) \\ (kL\cot(kL)-1)\csc(kL) & \big(\cot(kL) - kL\csc^2(kL)\big) \end{bmatrix}.$$

where $(\bullet)'$ is space first derivative.

Stochastic

The paper theory treats two different form to consider uncertainty in the stochastic model. The most used approaches to treat data uncertainty are like random variables or random processes [49]. When the uncertainty is considered as the random variable we used the Monte Carlo simulation and as a random process applied the Karhunen-Loève (KL) expansion decomposition. In the section demonstrate the developed stochastic model for damaged and undamaged rods in axial vibration combining (KL) expansion and Spectral Element Method.

The random field is discretized in terms of random variables. By doing this, many mathematical procedures can be used to solve the resulting discrete stochastic differential equations. The procedure applied here is a random field spectral decomposition using the Karhunen-Loève (KL) expansion. In this paper, an approach has been applied to structural damage quantification. The random field is described by various points expressed by random variables, therefore, a large number of points is required for a good approximation. This concept

is similar to the Fourier series expansion. Assuming that the covariance function is bounded, symmetric and positive definite, it can be represented by a spectral decomposition. By using this concept a random field can be expressed as a generalised Fourier series,

$$\varpi(\mathbf{r},\theta) = \varpi_0(\mathbf{r}) + \sum_{j=1}^{\infty} \xi_j(\theta)\sqrt{\lambda_j}\varphi_j(\mathbf{r}) \tag{11}$$

where $\varpi(\mathbf{r},\theta)$ is a random field with the covariance function $C_{\varpi}(\mathbf{r}_1,\mathbf{r}_2)$ defined in a space $\mathcal{D}$. Here θ denotes an element of the sample space Ω, so that $\theta \in \Omega$; $\xi_j(\theta)$ are uncorrelated random variables. The subscript 0, $\varpi_0(\mathbf{r})$, implies the corresponding deterministic part. The constants λ_j and functions $\varphi_j(\mathbf{r})$ are, respectively, eigenvalues and eigenfunctions satisfying the integral equation

$$\int_{\mathcal{D}} C_{\varpi}(\mathbf{r}_1,\mathbf{r}_2)\varphi_j(\mathbf{r}_1)d\mathbf{r}_1 = \lambda_j\varphi_j(\mathbf{r}_2) \quad \forall j = 1,2,....$$

In this paper, one dimensional space is considered. Since a Gaussian random field is representative of many physical systems and closed form expressions for the KL expansion may be obtained, then a Gaussian autocorrelation function with exponential decaying will be used. It can be expressed as,

$$C(x_1,x_2) = e^{-|x_1-x_2|/\mathtt{b}} \tag{12}$$

where ($\mathtt{b} > 0$) is the correlation length, which is an important parameter to describe the random field. A random field becomes a random variable if the correlation length is large as compared with the domain under consideration. An analytical solution in the interval $-\mathtt{a} < x < \mathtt{a}$ where it is assumed that the mean is zero, produces a random field as

$$\varpi_1(x,\theta) = \sum_{j=1}^{\infty} \xi_j(\theta)\sqrt{\lambda_j}\varphi_j(x) \tag{13}$$

Defining that $\mathtt{c} = 1/\mathtt{b}$, the corresponding eigenvalues and eigenfunctions for odd j are given by [50],

$$\lambda_j = \frac{2\mathtt{c}}{\omega_j^2 + \mathtt{c}^2}; \quad \varphi_j(x)\frac{\cos(\omega_j x)}{\sqrt{\mathtt{a} + \frac{\sin(2\omega_j \mathtt{a})}{2\omega_j}}} \qquad \text{where} \quad \tan(\omega_j \mathtt{a}) = \frac{\mathtt{c}}{\omega_j} \tag{14}$$

and for even j are given by,

$$\lambda_j = \frac{2\mathtt{c}}{\omega_j^2 + \mathtt{c}^2}; \quad \varphi_j(x)\frac{\sin(\omega_j x)}{\sqrt{\mathtt{a} - \frac{\sin(2\omega_j \mathtt{a})}{2\omega_j}}} \qquad \text{where} \quad \tan(\omega_j \mathtt{a}) = \frac{\omega_j}{-\mathtt{c}} \tag{15}$$

for $x = L/2$. These eigenvalues and eigenfunctions will be used to obtain the stochastic dynamic stiffness matrices for undamaged and damaged rod spectral elements.

For practical applications, the eq. (13) is truncated with N numbers of terms, which could be selected based on the amount of information to be kept. Its value is also related to the correlation length and the number of eigenvalues kept, provided that they are arranged in decreasing order [27]. In KL assumption, the processes is an underlying Gaussian. However, it is not applicable for most of the physical systems which, on the contrary, are expected to be characterised by nonlinear behaviours [53]. In this paper will consider the problem of the numerical simulation of non-Gaussian. Based on the assumption of the KL expansion a non-Gaussian process is expressed as a memoryless transformation of an underlying Gaussian process. The covariance function $C(x_1, x_2)$ of the underlying Gaussian process is chosen so that the transformation leads to a non-Gaussian process with the proposed covariance function $Cs(x_1, x_2)$. A non-Gaussian process $\varpi(x, \theta)$ is expressed as a memoryless transformation of an underlying standard Gaussian process $Z(\mathbf{x}, \theta)$ by means of the cumulative density functions (CDF) of both processes:

$$\varpi(\mathbf{x}, \theta) = F_{\varpi x}^{-1}(F_Z(Z(\mathbf{x}, \theta))) \tag{16}$$

where $F_{\varpi x}(\varpi)$is the marginal CDF of the non-Gaussian process and $F_Z(z)$ is the standard Gaussian CDF. An approximation of the transformation can be obtained in terms of the one-dimensional Hermite polynomials of order P:

$$\varpi(\mathbf{x}, \theta) \approx \sum_{n=0}^{P} a_n(\mathbf{x}) h_n(Z(\mathbf{x}, \theta))) \tag{17}$$

The coefficients $\{a_n(x)\}_n$ are obtained based on orthonormality of the Hermite polynomials $\{h_n(z)\}_n$ [59, 60] and a stationary process, it can be expressed as:

$$a_n(\mathbf{x}) = \int_{\infty}^{\infty} F_{Yx}^{-1}(F_Z(z)) h_n(z) \mathtt{p}_Z(z) dz \tag{18}$$

Equating the covariance of eq. 16 leads to:

$$Cs(\mathbf{x}_1, \mathbf{x}_2) \approx \sum_{n=0}^{P} a_n(\mathbf{x}_1) a_n(\mathbf{x}_2) [C(\mathbf{x}_1, \mathbf{x}_2)]^n \tag{19}$$

If $\varpi(\mathbf{x}, \theta)$ is a stationary process, then the covariance can be reduces to:

$$Cs(\Delta\mathbf{x}) \approx \sum_{n=0}^{P} a_n^2 [C(\Delta\mathbf{x})]^n \tag{20}$$

The same undamaged rod analytical model considered in the deterministic formulation is used here for the stochastic formulation. Now it is assumed that cross-section area, mass density, and Young's modulus are random variables spatially distributed. Therefore, the longitudinal rigidity (EA) and mass per unit of length (ρA) are assumed as a random field respectively of the form

$$EA(x, \theta) = EA_0[1 + \varepsilon_1 \varpi_1(x, \theta)]; \qquad \rho A(x, \theta) = \rho A_0[1 + \varepsilon_2 \varpi_2(x, \theta)] \tag{21}$$

where the subscript 0 indicates the underlying baseline model and ε_i are deterministic constants ($0 < \varepsilon_i \ll 1, i = 1, 2$). The random fields $\varpi_i(x, \theta), i = 1, 2$ are taken to have zero mean, unit standard deviation and covariance $C_{ij}(\xi)$. Since, $EA(x, \theta)$ and $\rho A(x, \theta)$ are strictly positive, $\varpi_i(x, \theta)$ are required to satisfy the probability condition $\mathrm{P}[1 + \varepsilon_i \varpi_i(x, \theta) \leq 0] = 0$. To obtain the stiffness and mass matrices associated with the random components, for each j, two different matrices correspond to the two eigenfunctions defined in eqs. (14) and (15) as

$$\mathbf{K}(\omega, \theta) = \mathbf{K}_0(\omega) + \Delta\mathbf{K}(\omega, \theta); \qquad \mathbf{M}(\omega, \theta) = \mathbf{M}_0(\omega) + \Delta\mathbf{M}(\omega, \theta) \tag{22}$$

where $\Delta\mathbf{K}_e(\omega, \theta)$ and $\Delta\mathbf{M}_e(\omega, \theta)$ are the random part of the stiffness and mass matrices. From the KL expansion and eqs. (21), this matrices can be conveniently expressed as,

$$\Delta\mathbf{K}(\omega, \theta) = \varepsilon_1 \sum_{j=1}^{N} \xi_{Kj}(\theta) \sqrt{\lambda_{Kj}} \mathbf{K}_j(\omega); \qquad \Delta\mathbf{M}(\omega, \theta) = \varepsilon_2 \sum_{j=1}^{N} \xi_{Mj}(\theta) \sqrt{\lambda_{Mj}} \mathbf{M}_j(\omega) \tag{23}$$

where N is the number of terms kept in the KL expansion, $\xi_{Kj}(\theta)$ and $\xi_{Mj}(\theta)$ are uncorrelated Gaussian random variables with zero mean and unit standard

deviation. The matrices $\mathbf{K}_j(\omega)$ and $\mathbf{M}_j(\omega)$ are written as

$$\mathbf{K}_j(\omega) = EA_0\mathbf{\Gamma}^T(\omega)\left[\int_0^L \varphi_{Kj}(x_e+x)\mathbf{s}'(x,\omega)^T\mathbf{s}'(x,\omega)dx\right]\mathbf{\Gamma}(\omega), \tag{24}$$

$$\mathbf{M}_j(\omega) = \rho A_0\mathbf{\Gamma}^T(\omega)\left[\int_0^L \varphi_{Mj}(x_e+x)\mathbf{s}(x,\omega)^T\mathbf{s}(x,\omega)dx\right]\mathbf{\Gamma}(\omega), \tag{25}$$

Substituting eqs. (14) and (15) in eqs. (24) the random part of the dynamic stiffness element matrix in a closed-form expressions with odd j is

$$\mathbf{K}_j^{odd}(\omega) = \frac{EA_0}{\sqrt{\mathtt{a}+\frac{\sin(2w_j\mathtt{a})}{2w_j}}}\mathbf{\Gamma}^T(\omega)\left[\int_0^L \cos(\omega_j(x_e+x))\mathbf{s}'(x,\omega)^T\mathbf{s}'(x,\omega)dx\right]\mathbf{\Gamma}(\omega)$$

$$= \frac{EA_0}{\sqrt{\mathtt{a}+\frac{\sin(2w_j\mathtt{a})}{2w_j}}}\begin{bmatrix} Ko_{11} & Ko_{12} \\ Sym & Ko_{22}\end{bmatrix} \tag{26}$$

$$\mathbf{M}_j^{odd}(\omega) = \frac{\rho A_0}{\sqrt{\mathtt{a}+\frac{\sin(2w_j\mathtt{a})}{2w_j}}}\mathbf{\Gamma}^T(\omega)\left[\int_0^L \cos(\omega_j(x_e+x))\mathbf{s}(x,\omega)^T\mathbf{s}(x,\omega)dx\right]\mathbf{\Gamma}(\omega)$$

$$= \frac{\rho A_0}{\sqrt{\mathtt{a}+\frac{\sin(2w_j\mathtt{a})}{2w_j}}}\begin{bmatrix} Mo_{11} & Mo_{12} \\ Sym & Mo_{22}\end{bmatrix} \tag{27}$$

and for even j it is given by,

$$\mathbf{K}_j^{even}(\omega) = \frac{EA_0}{\sqrt{\mathtt{a}-\frac{\sin(2w_j\mathtt{a})}{2w_j}}}\mathbf{\Gamma}^T(\omega)\left[\int_0^L \sin(\omega_j(x_e+x))\mathbf{s}'(x,\omega)^T\mathbf{s}'(x,\omega)dx\right]\mathbf{\Gamma}(\omega)$$

$$= \frac{EA_0}{\sqrt{\mathtt{a}-\frac{\sin(2w_j\mathtt{a})}{2w_j}}}\begin{bmatrix} Ke_{11} & Ke_{12} \\ Sym & Ke_{22}\end{bmatrix} \tag{28}$$

$$\mathbf{M}_j^{even}(\omega) = \frac{\rho A_0}{\sqrt{\mathtt{a}-\frac{\sin(2w_j\mathtt{a})}{2w_j}}}\mathbf{\Gamma}^T(\omega)\left[\int_0^L \sin(\omega_j(x_e+x))\mathbf{s}(x,\omega)^T\mathbf{s}(x,\omega)dx\right]\mathbf{\Gamma}(\omega)$$

$$= \frac{\rho A_0}{\sqrt{\mathtt{a}-\frac{\sin(2w_j\mathtt{a})}{2w_j}}}\begin{bmatrix} Me_{11} & Me_{12} \\ Sym & Me_{22}\end{bmatrix} \tag{29}$$

The exact closed-form expression of the elements, $Ko_{ij}, Mo_{ij}, Ke_{ij}, Me_{ij}$, of these four matrices (eqs. 26 to 29) are given in Appendix Appendix A.1.

Substituting eqs. (26 to 29) into the eqs. (22 the stochastic spectral undamaged rod element stiffness and mass matrices, $\mathbf{K}(\omega, \theta)$ and $\mathbf{M}(\omega, \theta)$, can be obtained. And then, the stochastic spectral undamaged rod element dynamic stiffness matrix is obtained as:

$$\mathbf{D}(\omega, \theta) = \mathbf{K}(\omega, \theta) - \omega^2 \mathbf{M}(\omega, \theta) \tag{30}$$

2.2. Damaged rod

Deterministic

This section presents the formulation for a spectral rod element with a transverse, open and non-propagating crack [3, 61]. Figure 2 shows a two-nodes rod element with uniform rectangular cross-section, length L, crack position L_1, crack depth α. The crack is modelled as a dimensionless and local crack flexibility, Θ, which is calculated by Castigliano's theorem and the laws of fracture mechanics [62].

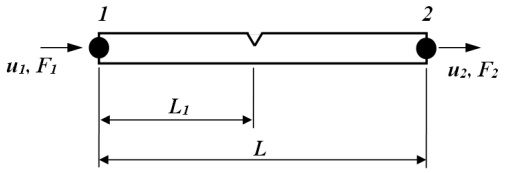

Figure 2: Two-node damaged rod spectral element

The homogeneous displacement solution for eq. (1) applied for this element must be described in two parts, one for the left-hand side of the crack and other for the right-hand side of the crack.

$$\begin{aligned} u_L(x) &= a_1 e^{-ikx} + a_2 e^{-ik(L_1 - x)} \qquad (0 \leq x \leq L_1) \\ &= \mathbf{s}_L(x; \omega)\mathbf{a}_L, \end{aligned} \tag{31}$$

where $\mathbf{s}_L(x,\omega) = [e^{-ikx}\ e^{-ik(L_1-x)}]$; and $\mathbf{a}_L = \{a_1\ a_2\}^T$.

$$u_R(x) = a_3 e^{-ik(x+L_1)} + a_4 e^{-ik[L-(L_1+x)]} \qquad (0 \le x \le L - L_1) \qquad (32)$$
$$= \mathbf{s}_R(x;\omega)\mathbf{a}_R,$$

where $\mathbf{s}_R(x,\omega) = [e^{-ik(x+L_1)}\ e^{-ik[L-(L_1+x)]}$; and $\mathbf{a}_R = \{a_3\ a_4\}^T$. Writing the eq. (31) and (32) in matrix form it has,

$$\left\{ \begin{array}{c} u_L(x) \\ u_R(x) \end{array} \right\} = \left[\begin{array}{cc} \mathbf{s}_L(x,\omega) & \mathbf{0} \\ \mathbf{0} & \mathbf{s}_R(x,\omega) \end{array} \right] \left\{ \begin{array}{c} \mathbf{a}_L \\ \mathbf{a}_R \end{array} \right\} = \mathbf{s}_d(x,\omega)\mathbf{a}_d \qquad (33)$$

The coefficients vector $\mathbf{a}_d$ can be calculated as a function of the nodal spectral displacements using the element boundary and compatibility conditions at the element left-end $u_L(0) = u_1$; at the element non-cracked cross-section$u_L(L_1) - u_R(0) = \Theta\partial u/\partial x$; at the element non-cracked cross-section $\partial u_L(L_1)/\partial x = \partial u_R(0)/\partial x$; and at the element right-end $u_R(L - L_1) = u_2$ Coupling the damaged element left and right-hand sides (eqs. 31 and 32) and applying boundary and compatibility conditions it has,

$$\underbrace{\left[\begin{array}{cccc} 1 & e^{-ikL_1} & 0 & 0 \\ (ik\Theta - 1)e^{-ikL_1} & (ik\Theta - 1) & e^{-ikL_1} & e^{-ik(L-L_1)} \\ -ike^{-ikL_1} & ik & ike^{-ikL_1} & -ike^{-ik(L-L_1)} \\ 0 & 0 & e^{-ikL} & 1 \end{array} \right]}_{\mathbf{G}_d} \left\{ \begin{array}{c} a_1 \\ a_2 \\ a_3 \\ a_4 \end{array} \right\} = \left\{ \begin{array}{c} u_1 \\ 0 \\ 0 \\ u_2 \end{array} \right\} \qquad (34)$$

where $\mathbf{G}_{dr}^{-1}$ reduced in the elements nodes is given by

$$\mathbf{G}_d^{-1} = \left[\begin{array}{cc} \frac{e^{ikL_1}((k\Theta - i)\cos(k(L-L_1)) + \sin(k(L-L_1)))}{k\Theta(\cos(kL)+\cos(k(L-2L_1)))+2\sin(kL)} & \frac{i}{k\Theta(\cos(kL)+\cos(k(L-2L_1)))+2\sin(kL)} \\ \frac{(k\Theta + i)\cos(k(L-L_1)) + \sin(k(L-L_1))}{k\Theta(\cos(kL)+\cos(k(L-2L_1)))+2\sin(kL)} & -\frac{ie^{ikL_1}}{k\Theta(\cos(kL)+\cos(k(L-2L_1)))+2\sin(kL)} \\ -\frac{ie^{ikL}}{k\Theta(\cos(kL)+\cos(k(L-2L_1)))+2\sin(kL)} & \frac{\left(1+e^{2ikL_1}\right)k\Theta+2i}{2k\Theta(\cos(kL)+\cos(k(L-2L_1)))+4\sin(kL)} \\ \frac{i}{k\Theta(\cos(kL)+\cos(k(L-2L_1)))+2\sin(kL)} & \frac{e^{ik(L-L_1)}((k\Theta - i)\cos(kL_1)+\sin(kL_1))}{k\Theta(\cos(kL)+\cos(k(L-2L_1)))+2\sin(kL)} \end{array} \right] \qquad (35)$$

Equation (34) can be rewritten in a compact form as $\mathbf{a}_d = \mathbf{G}_{dr}^{-1}\mathbf{d}_d$ as

$$\left\{ \begin{array}{c} u_L(x) \\ u_R(x) \end{array} \right\} = \left[\begin{array}{cc} \mathbf{s}_L(x,\omega) & \mathbf{0} \\ \mathbf{0} & \mathbf{s}_R(x,\omega) \end{array} \right] \mathbf{G}_{dr}^{-1}\mathbf{d}_d = \mathbf{g}_d(x,\omega)\mathbf{d}_d \qquad (36)$$

where $\mathbf{\Gamma}_d(\omega) = \mathbf{G}_{dr}^{-1}$.

For the damaged rod model, the stiffness matrix must be integrated according to the corresponding limits due the spacial reference in damaged model to be different for left-hand side and right-hand side of the crack position, then

$$\mathbf{K}_{0_d}(\omega) = EA_0\ \mathbf{\Gamma}_d^T(\omega) \begin{bmatrix} \int_0^{L_1} \mathbf{s'}_L^T(x,\omega)\mathbf{s'}_L(x,\omega)dx & \mathbf{0} \\ \mathbf{0} & \int_0^{(L-L_1)} \mathbf{s'}_R^T(x,\omega)\mathbf{s'}_R(x,\omega)dx \end{bmatrix} \mathbf{\Gamma}_d(\omega),$$

$$= \begin{bmatrix} K_{0d_{11}} & K_{0d_{12}} \\ sym & K_{0d_{22}} \end{bmatrix} \tag{37}$$

Similarly, the damage rod deterministic mass element matrix is obtained as:

$$\mathbf{M}_{0_d}(\omega) = \rho A_0\ \mathbf{\Gamma}_d^T(\omega) \begin{bmatrix} \int_0^{L_1} \mathbf{s}_L^T(x,\omega)\mathbf{s}_L(x,\omega)dx & \mathbf{0} \\ \mathbf{0} & \int_0^{(L-L_1)} \mathbf{s}_R^T(x,\omega)\mathbf{s}_R(x,\omega)dx \end{bmatrix} \mathbf{\Gamma}_d(\omega),$$

$$= \begin{bmatrix} M_{0d_{11}} & M_{0d_{12}} \\ sym & M_{0d_{22}}. \end{bmatrix} \tag{38}$$

The exact closed-form expression of the elements, $K_{0d_{ij}}$ and $M_{0d_{ij}}$, of these two matrices (eqs. 37 to 38) are given in Appendix Appendix B.1.

Stochastic

Likewise the stochastic undamaged rod formulation, the stochastic dynamic stiffness element matrix for the damaged rod spectral element, $\mathbf{D}_d(\omega,\theta)$, is developed. The same damaged rod analytical model considered in the deterministic formulation is used here for the stochastic formulation. Also, it is assumed that A, E, ρ are random variables, and EA and ρA are random fields. We can express the stochastic damaged rod stiffness and mass element matrices, respectively, as:

$$\mathbf{K}_d(\omega,\theta) = \mathbf{K}_{0_d}(\omega) + \Delta\mathbf{K}_d(\omega,\theta); \qquad \mathbf{M}_d(\omega,\theta) = \mathbf{M}_{0_d}(\omega) + \Delta\mathbf{M}_d(\omega,\theta) \tag{39}$$

From the KL expansion and eqs. (21) it has,

$$\Delta\mathbf{K}_d(\omega,\theta) = \varepsilon_1 \sum_{j=1}^{N} \xi_{Kj}(\theta)\sqrt{\lambda_{Kj}}\mathbf{K}_{j_d}(\omega); \qquad \Delta\mathbf{M}_d(\omega,\theta) = \varepsilon_2 \sum_{j=1}^{N} \xi_{Mj}(\theta)\sqrt{\lambda_{Mj}}\mathbf{M}_{j_d}(\omega) \tag{40}$$

where N is the number of terms kept in the KL expansion, $\xi_{Kj}(\theta)$ and $\xi_{Mj}(\theta)$ are uncorrelated Gaussian random variables with zero mean and unit standard deviation. By considering different limits of integration (left and right-hand sides) for the damaged rod model it has,

$$\mathbf{K}_{j_d}(\omega) = EA_0\mathbf{\Gamma}_d^T(\omega)\begin{bmatrix} \mathbf{Sk}_L & \mathbf{0} \\ \mathbf{0} & \mathbf{Sk}_R \end{bmatrix}\mathbf{\Gamma}_d(\omega), \tag{41}$$

$$\mathbf{M}_{j_d}(\omega) = \rho A_0\mathbf{\Gamma}_d^T(\omega)\begin{bmatrix} \mathbf{Sm}_L & \mathbf{0} \\ \mathbf{0} & \mathbf{Sm}_R \end{bmatrix}\mathbf{\Gamma}_d(\omega), \tag{42}$$

where

$$\begin{aligned}
\mathbf{Sk}_L &= \int_0^{L_1} \varphi_{Kj}(x_e+x)\mathbf{s'}_L^T(x,\omega)\mathbf{s'}_L(x,\omega)dx \\
\mathbf{Sk}_R &= \int_0^{(L-L_1)} \varphi_{Kj}(x_e+x)\mathbf{s'}_R^T(x,\omega)\mathbf{s'}_R(x,\omega)dx \\
\mathbf{Sm}_L &= \int_0^{L_1} \varphi_{Mj}(x_e+x)\mathbf{s}_L^T(x,\omega)\mathbf{s}_L(x,\omega)dx \\
\mathbf{Sm}_R &= \int_0^{(L-L_1)} \varphi_{Mj}(x_e+x)\mathbf{s}_R^T(x,\omega)\mathbf{s}_R(x,\omega)dx
\end{aligned} \tag{43}$$

Substituting eqs. (14) and (15) in eqs. (43) the random part of the stiffness and mass matrices as closed-form expressions can be obtained. However, these are huge closed-form expressions not easily workable. Then, eqs. (41) and (42) were solved with MATHEMATICA® software and exported directly to the MATLAB® code to obtain the numerical solutions. As a matter of understanding and results in reproducibility it is shown here only the matrices form of $\mathbf{Sk}_L, \mathbf{Sk}_R, \mathbf{Sm}_L, \mathbf{Sm}_R$ for each j^{th} terms respecting the odd and even KL formulation. By considering odd j it has,

$$\mathbf{Sk}_L^{odd}(\omega) = \frac{EA_0}{\sqrt{\mathtt{a} + \frac{\sin(2w_j\mathtt{a})}{2w_j}}}\begin{bmatrix} SkLo_{11} & SkLo_{12} \\ Sym & SkLo_{22} \end{bmatrix}$$

$$\mathbf{Sk}_R^{odd}(\omega) = \frac{EA_0}{\sqrt{\mathtt{a} + \frac{\sin(2w_j\mathtt{a})}{2w_j}}}\begin{bmatrix} SkRo_{11} & SkRo_{12} \\ Sym & SkRo_{22} \end{bmatrix}$$

$$\mathbf{Sm}_L^{odd}(\omega) = \frac{\rho A_0}{\sqrt{\mathtt{a} + \frac{\sin(2w_j\mathtt{a})}{2w_j}}} \begin{bmatrix} SmLo_{11} & SmLo_{12} \\ Sym & SmLo_{22} \end{bmatrix}$$

$$\mathbf{Sm}_R^{odd}(\omega) = \frac{\rho A_0}{\sqrt{\mathtt{a} + \frac{\sin(2w_j\mathtt{a})}{2w_j}}} \begin{bmatrix} SmRo_{11} & SmRo_{12} \\ Sym & SmRo_{22} \end{bmatrix} \tag{44}$$

and for even j it has,

$$\mathbf{Sk}_L^{even}(\omega) = \frac{EA_0}{\sqrt{\mathtt{a} - \frac{\sin(2w_j\mathtt{a})}{2w_j}}} \begin{bmatrix} SkLe_{11} & SkLe_{12} \\ Sym & SkLe_{22} \end{bmatrix}$$

$$\mathbf{Sk}_R^{even}(\omega) = \frac{EA_0}{\sqrt{\mathtt{a} - \frac{\sin(2w_j\mathtt{a})}{2w_j}}} \begin{bmatrix} SkRe_{11} & SkRe_{12} \\ Sym & SkRe_{22} \end{bmatrix}$$

$$\mathbf{Sm}_L^{even}(\omega) = \frac{\rho A_0}{\sqrt{\mathtt{a} - \frac{\sin(2w_j\mathtt{a})}{2w_j}}} \begin{bmatrix} SmLe_{11} & SmLe_{12} \\ Sym & SmLe_{22} \end{bmatrix}$$

$$\mathbf{Sm}_R^{even}(\omega) = \frac{\rho A_0}{\sqrt{\mathtt{a} - \frac{\sin(2w_j\mathtt{a})}{2w_j}}} \begin{bmatrix} SmRe_{11} & SmRe_{12} \\ Sym & SmRe_{22} \end{bmatrix} \tag{45}$$

The exact closed-form expression of each element, $\{SkLo_{ij}, SmLo_{ij}, SkRo_{ij}, SmRo_{ij}\}$ and $\{SkLe_{ij}, SmLe_{ij}, SkRe_{ij}, SmRe_{ij}\}$, of these eight matrices are given in Appendix Appendix B.2.

Crack flexibility

The crack flexibility coefficient (Θ) is calculated using Castigliano's theorem, where the flexibility at the crack location for the one-dimensional rod spectral element is obtained as in [62, 63]. Figure 3 shows the damaged rod element cross-section at the crack position, including the new geometric definition of crack depth as $\alpha = a/h$. The crack flexibility coefficient is written as a function of crack depth as,

$$\mathtt{c}(\alpha) = \frac{2\pi}{Eb} \int_0^{\alpha} \alpha \mathtt{f}(\alpha)^2 d\alpha,$$

where the function $\mathtt{f}$ is given by,

$$\mathtt{f}(\alpha) = 1.122 - 0.231\alpha + 10.550\alpha^2 - 21.710\alpha^3 + 30.382\alpha^4.$$

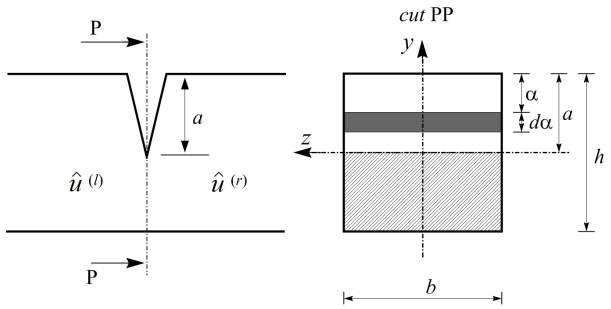

Figure 3: Damaged rod cross-section at the crack position

It can be shown that the dimensionless local crack flexibility can be written as

$$\Theta = 2\pi h \int_0^{\alpha} \alpha \mathtt{f}(\alpha)^2 d\alpha \tag{46}$$

3. Explicit crack detection

By solving the integral of eq. (46), the crack flexibility coefficient (Θ) can be expressed as

$$\Theta(\alpha) = 2\pi h(0.63\alpha^2 - 0.17\alpha^3 + 5.93\alpha^4 - 10.72\alpha^5 + 31.58\alpha^6 - 67.44\alpha^7 + 139.05\alpha^8 - 146.58\alpha^9 + 92.30\alpha^{10}) \tag{47}$$

Since the rod crack depth is a variable that physically quantifies the damage, it is important to find out an explicit equation to obtain α. Nevertheless, the dynamic spectral matrix for the damaged rod element (eq. 35) is a function of Θ, which in turn is a polynomial of degree 10 in α. To obtain a simple and feasible explicit solution for α, in this study a priori the crack flexibility polynomial is approximated by its first term. Figure 4 shows the crack flexibility coefficient calculated using polynomial with 2, 5, 7 and 10 degrees (eq. 47) versus different crack depths. For a crack depth until 0.13 the crack flexibility function with different degrees are practically the same. The divergence among the curves starts with a crack depth of 0.15 and increase as the crack depth increases.

In structural dynamic testing, it is a common practice to measure the data in the form of frequency response function (FRF). The knowledge about a par-

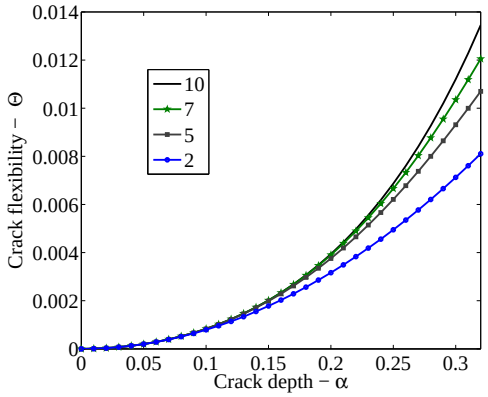

Figure 4: Crack flexibility coefficient versus crack depth for different polynomial degrees.

ticular structure will be contained in an analytical (or numerical) model. The theoretical FRF obtained from the analytical model here is the inverse of the dynamic stiffness matrix for structural systems. Many damage quantification methods use of comparing the undamaged with the damaged response of the system. One of them, called Damage Index (DI) define the average power reduction between the damaged and undamaged state signals [6]. Others authors [64, 65, 34, 66] proposed the percentage changes in the natural frequencies between the system undamaged and damaged states. Regarding this principle, we used a damage indicator defined by a *relative change* between the damaged and undamaged FRF's system

$$\mathbf{\Lambda}(\omega) = \frac{\mathbf{H}_d(\omega) - \mathbf{H}_u(\omega)}{\mathbf{H}_u(\omega)} \tag{48}$$

where $\mathbf{H}_d(\omega) = [\mathbf{K}_{d0}(\omega)]^{-1}$ is the damaged rod frequency response function (FRF), and $\mathbf{H}_u(\omega) = [\mathbf{K}_0(\omega)]^{-1}$ is the undamaged rod frequency response function, and ω is the frequency domain. Where $\mathbf{H}^{(\mathrm{ij})}$ is a FRF with response at node i and excitation at node j. The rod FRF matrix with respective terms can be obtained as,

$$\mathbf{H} = \begin{bmatrix} H^{(11)} & H^{(12)} \\ H^{(21)} & H^{(22)} \end{bmatrix} \tag{49}$$

To formulate the explicit equation, we started by considering a point receptance

FRF, e.g $\mathbf{H}^{(21)}$, for a damaged and undamaged rod models. The analytical and measured FRF are used to calculate the relative change as

$$\mathbf{\Lambda}_{an}(\omega) = \frac{\mathbf{H}^{(21)}_{d_{an}} - \mathbf{H}^{(21)}_{u_{an}}}{\mathbf{H}^{(21)}_{u_{an}}}, \quad \mathbf{\Lambda}_{m}(\omega) = \frac{\mathbf{H}^{(21)}_{d_{m}} - \mathbf{H}^{(21)}_{u_{m}}}{\mathbf{H}^{(21)}_{u_{m}}} \tag{50}$$

where measured FRF is the effect data which can be obtained experimentally or numerically, and the analytical FRF means the symbolic mathematical expression. The relative change using analytical FRF for a rod with two nodes is

$$\mathbf{\Lambda}_{an}(\omega) = \frac{\Theta k\left(-2\sin^2\left(k\left(L-L_1\right)\right) - \cos(kL) + \cos\left(k\left(L-2L_1\right)\right)\right)}{\left(\cos(kL)\right)\left(\Theta k\left(\cos(kL) - \cos\left(k\left(L-2L_1\right)\right)\right) - 2\sin(kL)\right)} \tag{51}$$

Similarly to the model updating approach, the inverse problem will be applied here as a technique where the structural damage parameter (α) will be quantified based on the minimization of the difference between analytical and measured FRF relative change [39, 40, 1] expressed by,

$$\mathbf{\Lambda}_{an}(\omega) - \mathbf{\Lambda}_{m}(\omega) = \varepsilon_{\mathbf{\Lambda}} \tag{52}$$

By neglecting modelling and measurements errors, so that $\varepsilon_{\Lambda} = 0$. The crack flexibility polynomial is approximated by its first term so that $\Theta = 2\pi h(0.63\alpha^2)$. Substituting eq. 51 in 52 and the consideration for ε_{Λ} and Θ it has

$$\frac{(2\pi h(0.63\alpha^2))k\left(-2\sin^2\left(k\left(L-L_1\right)\right) - \cos(kL) + \cos\left(k\left(L-2L_1\right)\right)\right)}{\left(\cos(kL)\right)\left((2\pi h(0.63\alpha^2))k\left(\cos(kL) - \cos\left(k\left(L-2L_1\right)\right)\right) - 2\sin(kL)\right)} - \mathbf{\Lambda}_{m}(\omega) = 0 \tag{53}$$

By using eq. (53) and solving into the MATHEMATICA software, the explicit equation for the crack depth ($\alpha(\omega)$) and crack position ($L_1(\omega)$) in function of the analytical and measured relative change is obtained. It have,

$$\alpha(\omega) = \frac{0.710812\sqrt{\mathbf{\Lambda}_m(\omega)\sin(2kL)}}{\sqrt{hk\mathbf{\Lambda}_m(\omega)[\cos(2kL) - \cos(2k(L-L_1)) - \cos(2kL_1)] - 2hk\cos(2k(L-L_1)) + hk\mathbf{\Lambda}_m(\omega) + 2hk}} \tag{54}$$

and crack position as

$$\mathbf{L_1}(\omega) = \left| \frac{2\theta k^3 L(\mathbf{\Lambda}_m(\omega)+1)(\cot(kL)-i) \pm 4i\csc^2(kL)\sqrt{\theta k^3(\mathbf{\Lambda}_m(\omega)+1)e^{-2ikL}\sin^2(kL)\left(\frac{1}{2}\theta k(\mathbf{\Lambda}_m(\omega)+1)(\cos(kL)-1) - \mathbf{\Lambda}_m(\omega)\sin(kL)\right)}}{4\theta k^3(\mathbf{\Lambda}_m(\omega)+1)(\cot(kL)-i)} \right| \tag{55}$$

The relative error between the crack depth calculated with the eq. (47) and with the approximation by its first term and the relative error between the crack position calculated with the eq. (47) can be expressed by,

$$\varepsilon_{\alpha} = \left| \frac{\alpha_{no}(\omega) - \alpha_C(\omega)}{\alpha_{no}(\omega)} \right| \times 100, \qquad \varepsilon_{L_1} = \left| \frac{L_1^{no}(\omega) - L_1^C(\omega)}{L_1^{no}(\omega)} \right| \times 100$$

where nominal crack depth (α_{no}) is a given value at a nominal crack position L_1^{no}. It is used to obtain a measured FRF relative change (Λ_m) using the complete equation of crack flexibility (eq. 47). Then, Λ_m is substituted into eq. (54) and calculated the crack depth (α). By substituting α_{no}, α, L_1^{no}, and L_1 into the equation (56) the crack depth and crack position error in percentage are calculated.

3.1. Average crack depth and crack position estimation

In the procedure to estimate the crack depth (eq. 54) and crack position (eq. 55) presented in the Section 3, it will be required to obtain a measured FRF relative change. In this paper, the stochastic rod models calculate the measured FRF's to obtain $\Lambda_m(\omega, \theta)$ and three statistical approaches are used:

- Mathematical expectation of the measured FRF relative change, which can be expressed as,

$$\mathbf{\Lambda}_m^{(1)}(\omega) = \mathbb{E}\left[\frac{\mathbf{H}_{d_m}(\omega, \theta) - \mathbf{H}_{u_m}(\omega, \theta)}{\mathbf{H}_{u_m}(\omega, \theta)} \right] \tag{56}$$

- Mathematical expectation of the difference between measured damage and undamaged FRF's, divided by the mathematical expectation of the measured undamaged FRF. It can be expressed as,

$$\mathbf{\Lambda}_m^{(2)}(\omega) = \frac{\mathbb{E}[\mathbf{H}_{d_m}(\omega, \theta) - \mathbf{H}_{u_m}(\omega, \theta)]}{\mathbb{E}[\mathbf{H}_{u_m}(\omega, \theta)]} \tag{57}$$

- Mathematical expectation of the measured crack depth, $\mathbb{E}[\alpha(\omega)]$, calculated by,

$$\mathbf{\Lambda}_m^{(3)}(\omega, \theta) = \frac{\mathbf{H}_{d_m}(\omega, \theta) - \mathbf{H}_{u_m}(\omega, \theta)}{\mathbf{H}_{u_m}(\omega, \theta)} \tag{58}$$

using all samples of $\mathbf{H}_{d_m}(\omega, \theta)$ and $\mathbf{H}_{u_m}(\omega, \theta)$ generated by the stochastic process.

These three different ways to calculate the crack depth and position statistics were used because this is a non-linear problem. Thus, different results are expected for each formulation. An illustration of that non-linearity will be seen in Section 4.0.2, these results change in function of the frequency vary. Nevertheless, a physical crack reminds a single values, then these formulations are modified by integrating the measured FRF relative change ($\mathbf{\Lambda}_m$) over the frequency to estimate single value for α and L_1. By applying to the eqs. (56-58) we have:

$$\bar{\Lambda}_m^{(1)} = \int_\omega \mathbb{E}\left[\frac{\mathbf{H}_{d_m}(\omega,\theta) - \mathbf{H}_{u_m}(\omega,\theta)}{\mathbf{H}_{u_m}(\omega,\theta)}\right] d\omega \tag{59}$$

$$\bar{\Lambda}_m^{(2)} = \int_\omega \frac{\mathbb{E}[\mathbf{H}_{d_m}(\omega,\theta) - \mathbf{H}_{u_m}(\omega,\theta)]}{\mathrm{E}[\mathbf{H}_{u_m}(\omega,\theta)]} d\omega \tag{60}$$

and the third is obtained as $\int_\omega \mathbb{E}[\alpha(\omega)]d\omega$, which is the integral of the mathematical expectation of the measured crack depth, $\mathbb{E}\left[\alpha(\omega)\right]$, calculated by,

$$\bar{\Lambda}_m^{(3)}(\omega,\theta) = \frac{\mathbf{H}_{d_m}(\omega,\theta) - \mathbf{H}_{u_m}(\omega,\theta)}{\mathbf{H}_{u_m}(\theta)} \tag{61}$$

Next section shows a series of numerical and experimental cases to test the efficiency of the present study.

4. Numerical tests

4.0.1. Deterministic damage detection

The system consists of a free-free rod modelled with a two nodes spectral element. It is excited by a unit longitudinal harmonic force applied at the rod element node 1, and the response is obtained at node 2, figure 2. Geometries and material properties are: $L = 1.0$ m, $h = 0.018$ m, $b = 0.006$ m, $E = 71$ GPa, $\eta = 0.01$, and $\rho = 2700$ kg/m^3.

To verify the crack depth analytical expression (eq. 54), a measured FRF relative change (eq. 50) is obtained using the damage model with the crack flexibility (eq. 47), then substituted in the eq. 54. In pratical application the nominal crack depth values assumed are $\alpha_{no} = \{0.02, 0.10, 0.30\}$, at crack position value of $L_1 = 0.35L$. By introducing $\mathbf{\Lambda}_m$ in eq. 54, a crack depth (α)

is estimated. Figure 5 shows the calculated crack depth with the percentage relative error (eq. 56).

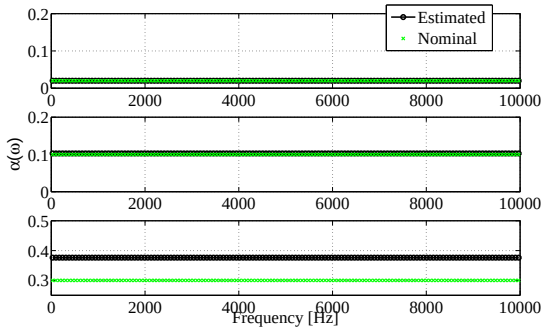

Figure 5: Estimation of crack depth for $\alpha_{no} = \{0.02, 0.10, 0.30\}$. Relative error ($\varepsilon_\alpha$) are equals to $0.1\%, 2.7\%$ and 21%, respectively.

The results show a good approximation in using the first term of eq. (47). The crack depth estimation with $\alpha_{no} = 0.30$ shows an error of 21%, it can be related to the reduction of the term in crack flexibility polynomial used to estimate α. The effect of the simplification adopted to obtain an explicit solution for α is showed in figure 4, as demonstrated a higher error was expected for crack depth above than 0.2. Although a crack depth of 30% of the high section is a quite considerable size, an efficient method such that to quantify a small to high crack size with accurate estimation. Based on the engineering point where the percentage errors (ε_α) until 20% is considerable acceptable, good crack depth estimation was obtained an increase of the polynomial degree is not considered.

Similar to crack depth tests, to verify the crack position analytical expression (eq. 55) and the sensibility of the crack position equation, the same measured FRF relative change is used. The nominal crack depth values assumed are $\alpha_{no} = \{0.02, 0.10, 0.30\}$ at crack position value of $L_1 = \{0.33L, 0.68L\}$. By introducing $\mathbf{\Lambda}_m$ in eq. 55 the crack positions are obtained. Figure 6 shows the estimated crack positions with the percentage relative error (eq. 56).

In all cases, good results with small error for L_1 were obtained independently of the crack depth. With regards to the uncertainty sources that a structure

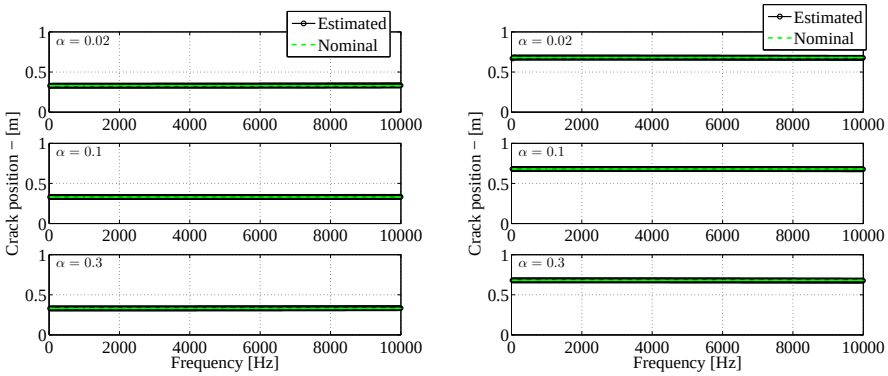

Figure 6: Crack position estimation in $L_1 = 0.33L$(left) and $0.68L$(right) for $\alpha = \{0.02, 0.10, 0.30\}$. Relative error ($\varepsilon_{L_1}$) are equals to $0.24\%, 0.25\%$ and 0.25%, respectively.

can contain, the following sections will be dedicated to verifying the efficiency of the present technique for damage detection considering a stochastic system.

4.0.2. Stochastic damage detection

To start with a numerical test depth crack estimation are considered stochastic dynamic responses for the undamaged and damage models. It was assumed a rod structure with the same geometries and material properties of the Section4.0.1. The crack depth value is of $\alpha_{no} = 0.10$ and crack positions is $L_1 = 0.3L$), where the rod length (L) now is 35 mm. The variability will be considered in cross section area and Young's modulus. For the random variable (RV) cases, both are assumed as a Gamma distribution with means, $\mu_A = 0.00096$ m^2 and $\mu_E = 71$ GPa, and coefficients of variation $COV_A = COV_E = \{0.01, 0.05, 0.1\}$. For the random field ($RF$) cases, the longitudinal rigidity $EA(x, \theta)$ has a Gamma marginal PDF. The covariance function of the random field is exponential with correlation length $\mathtt{b} = L/3$ and 4 modes. Monte Carlo simulation is evaluated with 500 samples. For the eqs. (56-58), $\mathbf{H}_{d_m}(\omega, \theta) = [\mathbf{K}_d(\omega, \theta)]^{-1}$ and $\mathbf{H}_{u_m}(\omega, \theta) = [\mathbf{K}(\omega, \theta)]^{-1}$.

Figure 7 shows the mean and standard deviation receptance FRF's for an undamaged rod, modelled as random variables (RV) with a damping factor of 0.01 and 0.05, and different COV's. Figure 9 shows the mean and standard de-

viation receptance FRF's for an undamaged rod, modelled as random variables (RF) with a damping factor of 0.01 and 0.05, and different COV's. For RV and RF cases, the mean responses are slightly different from the deterministic response. As the frequency and coefficient of variation increase, the stochastic responses presents an increasing damping behaviour. It comes from the average process which flattens curve peaks as the dispersion increases. These results agree with those presented in the literature by [67].

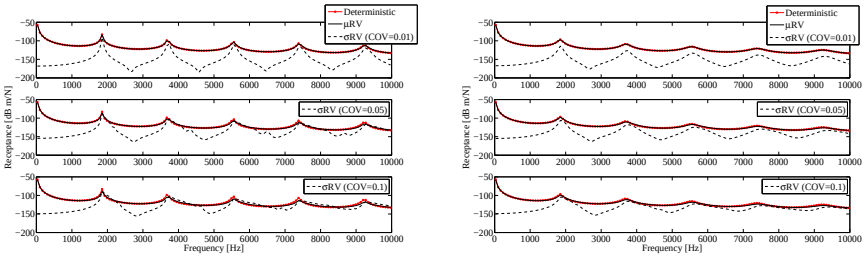

Figure 7: Mean receptance FRF ($\mathbf{H}^{12}$) and standard deviation for undamaged rod modelled by using RV with $\eta = 0.01$ (LHS) and $\eta = 0.05$ (RHS) for $COV = \{0.01, 0.05, 0.1\}$.

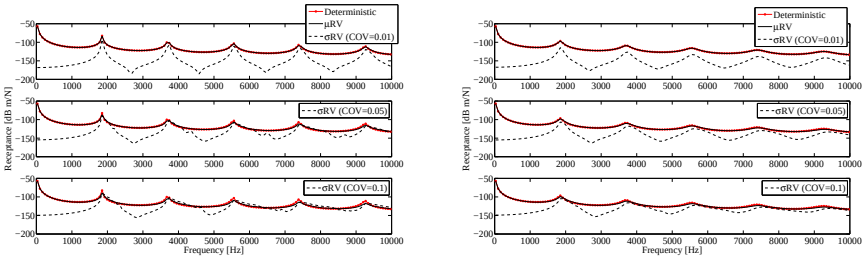

Figure 8: Mean receptance FRF ($\mathbf{H}^{12}$) and standard deviation for damaged rod modelled by using RV with $\eta = 0.01$ (LHS) and $\eta = 0.05$ (RHS) for $COV = \{0.01, 0.05, 0.1\}$.

For the damaged rod case the results presented similar behaviour as the undamaged model. Figure 8 shows the mean and standard deviation receptance FRF's for the damaged rod, modelled as random variables (RV) a with damping factor of 0.01 and 0.05 with different COV's. Figure 10 shows the mean and standard deviation receptance FRF's for the damaged rod, modelled as random variables (RF) with damping factor of 0.01 and 0.05 and different COV's.

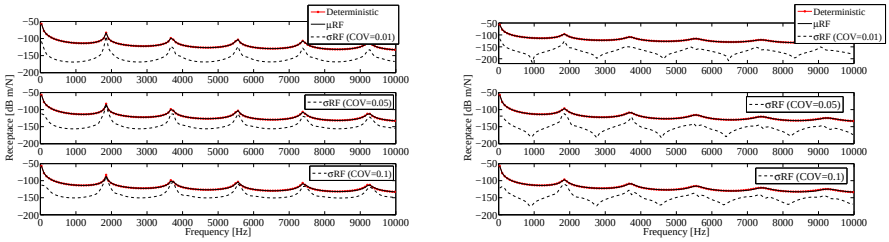

Figure 9: Mean receptance FRF ($\mathbf{H}^{12}$) and standard deviation for undamaged rod modelled by using RF with $\eta = 0.01$ (LHS) and $\eta = 0.05$ (RHS) for $COV = \{0.01, 0.05, 0.1\}$.

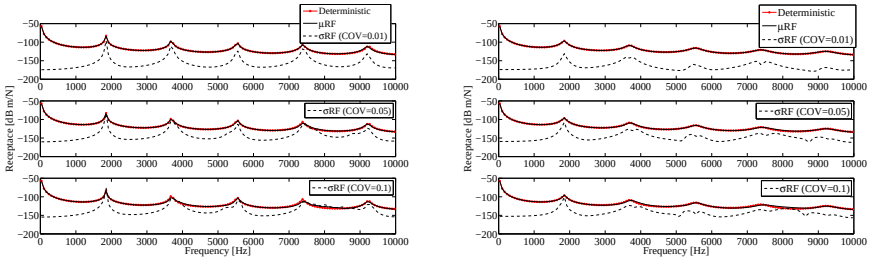

Figure 10: Mean receptance FRF ($\mathbf{H}^{12}$) and standard deviation for damaged rod modelled by using RF with $\eta = 0.01$ (LHS) and $\eta = 0.05$ (RHS) for $COV = \{0.01, 0.05, 0.1\}$.

Crack depth detection using random variables

By using the same numerical example, parameters variability, number of samples and measured FRF relative change as in the Section 4.0.2, the crack depth (α) is calculated by using random variable (RV) model in relation with $\mathbf{\Lambda}_m^{(1)}$, $\mathbf{\Lambda}_m^{(2)}$, and $\mathbf{\Lambda}_m^{(3)}$ (eqs. 56-58). By evaluating the structural damping effects on the stochastic damage quantification, two values of damping factor $\eta = 0.01$ and $\eta = 0.05$ are used.

Figure 11 shows the mean of crack depth for a given frequency band. By considering a damping factor $\eta = 0.01$ (LHS figure) with the low coefficient of variation ($COV = 1\%$), all approaches present good approximation between calculated and nominal crack depth. However, as the COV's increase α obtained by all approaches shows high dispersion around the value of α_{no} with $\Lambda_m^{(1)}$ and lower dispersion when compared to the others. By increasing the damping factor to $\eta = 0.05$ (RHS figure), the α converges to α_{no} much better, although it still has a moderate dispersion around the α_{no} at high values of COV. This comes

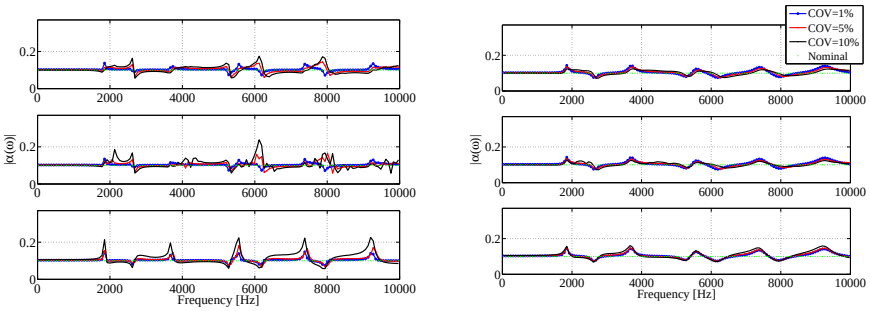

Figure 11: Mean of crack depth with RV model, for $COV = \{0.01, 0.05, 0.1\}$ using the approaches: $\Lambda_m^{(1)}$, $\Lambda_m^{(2)}$, and $\Lambda_m^{(3)}$, with damping factor $\eta = 0.01$ (LHS) and $\eta = 0.05$ (RHS).

from the fact that damping greatly influences the behaviour of the stochastic system [68, 69].

Likewise, figure 11 shows the mean of crack position detection in a given frequency band. By considering a damping factor $\eta = 0.01$ (LHS figure) and $\eta = 0.05$ (RHS figure) for all coefficient of variation values good approximation between calculated and nominal crack position are observed. The errors associated with the estimation are summarized in table 2.

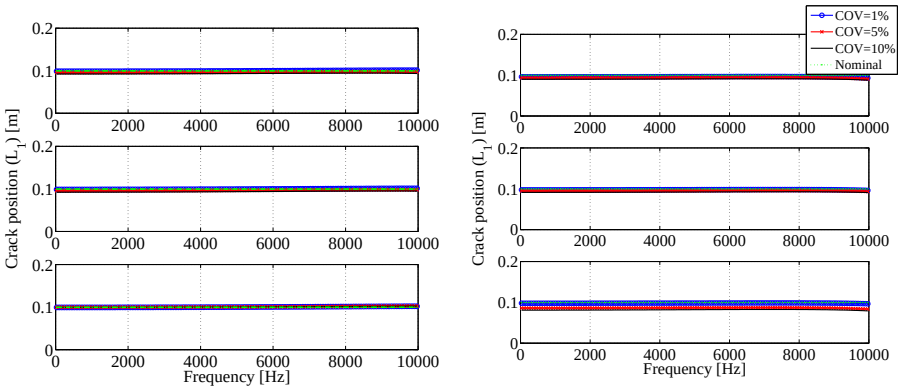

Figure 12: Mean of crack position with RV model, for $COV = \{0.01, 0.05, 0.1\}$ using the approaches: $\Lambda_m^{(1)}$, $\Lambda_m^{(2)}$, and $\Lambda_m^{(3)}$, with damping factor $\eta = 0.01$ (LHS) and $\eta = 0.05$ (RHS).

Thus, the result obtained from the RV model shows the influence of the different COV's where the ε_α increases as the COV increase when crack depth is estimated. While crack position estimation shows close estimation compared

with the nominal. Any influence of damping and small error are associated with the COV's increase. By comparing the three FRF relative change, $\mathbf{\Lambda}_1(\omega)$ exhibited the best outcome. With the increasing damping factor reduction of error is observed in all study cases, following the analogy, the error parameter increases with a higher coefficient of variation.

Crack depth detection using random field

By supposing that random material properties will change continuously over the structural space. In this situation the dynamic stiffness matrix for the two-node damaged and undamaged rod elements are modelled within the random field framework. By using the same numerical example, parameters variability, number of samples and measured FRF relative change as in the Section 4.0.2, the crack depth ($\alpha(\omega)$) calculated using RF model is based on the approaches $\mathbf{\Lambda}_m^{(1)}$, $\mathbf{\Lambda}_m^{(2)}$, and $\mathbf{\Lambda}_m^{(3)}$ (eqs. 56-58). Figure 13 illustrates nominal crack depth values and crack depth mean of the respective COV's for two values of damping factor ($\eta = 0.01$ and $\eta = 0.05$). In the response with damping factor $\eta = 0.01$

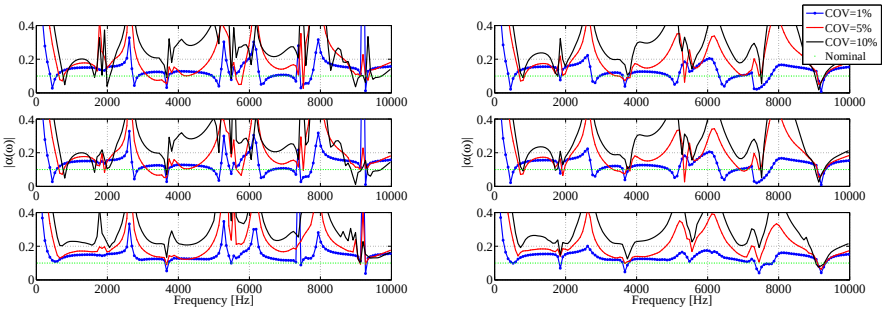

Figure 13: Mean of crack depth with RF model, for $COV = \{0.01, 0.05, 0.1\}$ using the approaches: $\mathbf{\Lambda}_m^{(1)}$, $\mathbf{\Lambda}_m^{(2)}$, and $\mathbf{\Lambda}_m^{(3)}$, with damping factor $\eta = 0.01$ (LHS) and $\eta = 0.05$ (RHS).

(LHS figure), mean of calculated crack depth (α) obtained with $\mathbf{\Lambda}_m^{(1)}(\omega)$ and $\mathbf{\Lambda}_m^{(2)}(\omega)$ shows better approximation to the nominal crack depth (α_{no}) when compared with other approaches. These results become better as the frequency rises and for small COV's. The means obtained with the approaches $\mathbf{\Lambda}_m^{(1)}(\omega, \theta)$ and $\mathbf{\Lambda}_m^{(2)}(\omega)$ present similar results for all values of COV's, with the α values

varying around (α_{no}) value. Based on the results, it can be seen that the crack depth estimation presents a great oscillation due to the randomness in wave numbers. Also, like the random variable case, as the damping factor increases, the calculated crack depth responses approximates more to the nominal crack depth value.

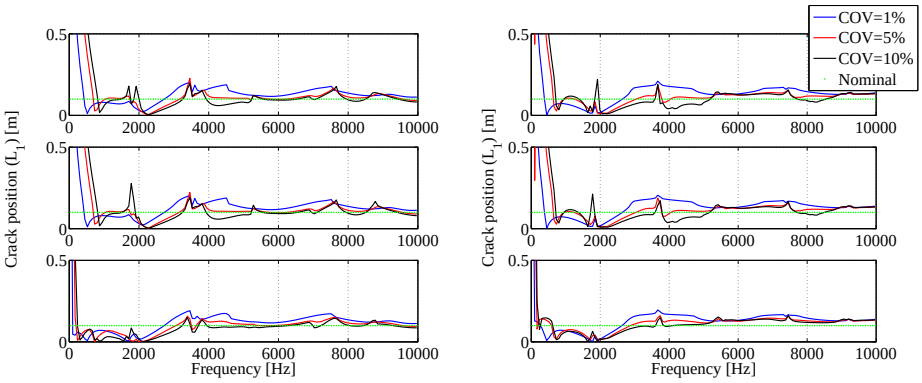

Figure 14: Mean of crack position with RF model, for $COV = \{0.01, 0.05, 0.1\}$ using the approaches: $\mathbf{\Lambda}_m^{(1)}$, $\mathbf{\Lambda}_m^{(2)}$, and $\mathbf{\Lambda}_m^{(3)}$, with damping factor $\eta = 0.01$ (LHS) and $\eta = 0.05$ (RHS).

Figure 14 illustrates nominal crack position values and crack position mean of the respective COV's for two values of damping factor ($\eta = 0.01$ and $\eta = 0.05$). Like the random variable case, the damping do not have great influence in the damage location as in damage quantification case. Herein, the damping effects is lightly visible for small COVs. Crack position estimation using $\mathbf{\Lambda}_m^{(1)}(\omega)$, $\mathbf{\Lambda}_m^{(2)}(\omega)$ and $\mathbf{\Lambda}_m^{(3)}(\omega)$ show a converge with to the nominal crack position (L_1^{no}) around 5500 Hz. The results for the crack depth and position in this section were obtained in the frequency domain. In the first analyse using a deterministic system, the crack depth and position values were constant along the frequency. However, in a stochastic model, it presented a random behaviour along the frequency. The crack depth showed high oscillations in the frequency domain, which in same cases became difficult to quantify the damage. The crack position presented oscillations in the frequency band $0 - 3700Hz$ and a convergence to the nominal values after 5500 Hz. in this case the damage location is suitable for all COV's analysed. For this reason, technique to obtain a single value for

the crack depth is presented in the next section.

4.0.3. Single crack depth detection

A single crack depth value was estimated using stochastic response obtained from RV and RF of the same numerical example. Parameter variability and a number of samples exposed in the previous cases. The measured FRF relative change are obtained by the eqs. (59-61). Predicted crack depth and crack depth error obtained for different approaches ($\bar{\Lambda}_m^{(1)}$, $\bar{\Lambda}_m^{(2)}$ and $\bar{\Lambda}_m^{(3)}$) are presented in Table 1.

Table 1: Calculated crack depth results using $\bar{\Lambda}_m^{(1)}$, $\bar{\Lambda}_m^{(2)}$, and $\bar{\Lambda}_m^{(3)}$ with $\alpha_{no} = 0.1$, modelled as RV and RF for different coefficient of variation (COV) and damping factor (η) values.

	COV	Calculated crack depth (Error ε_α [%])			
	[%]	$\eta = 0.01$		$\eta = 0.05$	
		RV	RF	RV	RF
$\bar{\Lambda}_m^{(1)}$	1	0.1027 (2.7)	0.1026 (2.6)	0.1016 (1.6)	0.1061 (6.1)
	5	0.1046 (4.6)	0.1419 (41.0)	0.1018 (1.8)	0.1277 (27.7)
	10	0.1055 (5.5)	0.1890 (89.0)	0.1023 (2.2)	0.1703 (70.3)
$\bar{\Lambda}_m^{(2)}$	1	0.1027 (4.0)	0.1026 (2.6)	0.1023 (2.3)	0.1061 (6.1)
	5	0.1055 (7.0)	0.1419 (41.0)	0.1021 (2.2)	0.1277 (27.7)
	10	0.1134 (11.0)	0.1890 (89.0)	0.1025 (2.5)	0.1703 (70.3)
$\bar{\Lambda}_m^{(3)}$	1	0.1031 (5.0)	0.1077 (7.66)	0.1030 (3.0)	0.1031 (3.05)
	5	0.1084 (11.0)	0.1816 (81.57)	0.1068 (6.8)	0.1588 (58.8)
	10	0.1128 (12.0)	0.2437 (143.7)	0.1097 (9.7)	0.2122 (112.2)

In the Table 1, it can be seen that for all COV's values with a damping factor $\eta = 0.01$ the calculated crack depths modelled as RV present crack depth error very low ($\varepsilon_\alpha = 4 - 11\%$). However, for the calculated crack depths modelled

as RF, these errors are high ($\varepsilon_\alpha = 6 - 86\%$). For all cases, ε_α increases as the coefficient of variation increases. Related with a greater damping factor ($\eta = 0.05$), and the RV model the ε_α presents almost the same value ($4.2-4.4\%$) for all COV's. For the RF model the ε_α presents similar results as obtained with $\eta = 0.01$, i.e. very high values for ε_α. Nonetheless, some conflicting results have been founded related with the COV, where with $\eta = 0.05$ for a $COV = 1\%$ the ε_α increases and for $COV = 5\%$ and 10% the ε_α decrease as compared with the results obtained with $\eta = 0.01$. It can be concluded that there are no significant differences in the approaches calculated with the equations of $\bar{\Lambda}_1$ and $\bar{\Lambda}_2$. Although the values of ε_α for $\bar{\Lambda}_3$ are higher than the ones of the other approaches. They do not present conflicting results for ε_α as the COV and η changes. Also, the results obtained confirms the expected behaviour, where ε_α should be increasing as COV increases, and in this case decreasing as η increases.

The crack position location and its error are also obtained with ($\bar{\Lambda}_m^{(1)}$, $\bar{\Lambda}_m^{(2)}$ and $\bar{\Lambda}_m^{(3)}$). The results are presented in Table 2. In all cases the crack position was located and the damping factor did not have a great influence in final results. The calculated crack position using the RV model presents low error ($\varepsilon_{L-1} = 0.01 - 1.9\%$) for small COV and ($\varepsilon_{L-1} = 5.9 - 9.9\%$) for high COV. The calculated crack positions using RF model had errors between ($\varepsilon_{L_1} = 1.2 - 29.8\%$). In all cases, ε_{L_1} increases as the coefficient of variation increases. Finally, there are no significant differences in the approaches calculated with $\bar{\Lambda}_1$ and $\bar{\Lambda}_2$. The values of ε_{L_1} for $\bar{\Lambda}_3$ are lightly different than the ones of the other approaches but it keeps good results. The results obtained confirms the expected behaviour, where ε_{L_1} should be increasing as COV increases.

To summarize, the damage quantification point of view crack depth calculated using the approach $\bar{\Lambda}_m^{(3)}$ with RV model presents a good performance. The α using the approaches $\bar{\Lambda}_m^{(1)}$ and $\bar{\Lambda}_m^{(2)}$ with RF model present some conflicting results as the damping factor increases, which requires more investigation. The

Table 2: Calculated crack position results using $\bar{\Lambda}_m^{(1)}$, $\bar{\Lambda}_m^{(2)}$, and $\bar{\Lambda}_m^{(3)}$ with $\alpha_{no} = 0.1$, modelled as RV and RF for different coefficient of variation (COV) and damping factor (η) values.

	COV	Calculated crack depth (Error ε_α [%])			
	[%]	$\eta = 0.01$		$\eta = 0.05$	
		RV	RF	RV	RF
$\bar{\Lambda}_m^{(1)}$	1	0.0996 (0.01)	0.0952 (4.4)	0.0976 (1.9)	0.0985 (1.2)
	5	0.0968 (2.8)	0.0869 (12.7)	0.0950 (4.6)	0.0876 (12.1)
	10	0.0968 (5.9)	0.0698 (29.8)	0.0917 (7.9)	0.0702 (29.5)
$\bar{\Lambda}_m^{(2)}$	1	0.0930 (0.01)	0.0965 (3.1)	0.0976 (1.9)	0.0968 (2.8)
	5	0.0997 (2.7)	0.0871 (12.5)	0.0950 (4.6)	0.0881 (11.6)
	10	0.0968 (5.6)	0.0699 (29.8)	0.0919 (7.7)	0.0702 (29.5)
$\bar{\Lambda}_m^{(3)}$	1	0.0933 (0.77)	0.0109 (9.5)	0.0979 (1.7)	0.010 (9.2)
	5	0.10 (4.5)	0.0115 (15.6)	0.0937 (5.9)	0.011 (14.7)
	10	0.0968 (7.77)	0.0128 (28.7)	0.0897 (9.9)	0.012 (24.7)

random field (RF) model reveals to be unable to estimate the crack depth (α) for high COV independently of the approach used to calculate the FRF relative change. Finally, the damage position calculated using the three approaches showed good performance and able to detect the damage with acceptable errors.

5. Conclusion

A stochastic damage quantification method is presented, which is developed combining Spectral Element Method (SEM) together with stochastic approaches using model parameters as random variables (RV) and spatially distributed random field (RF). Deterministic formulation for rod spectral element undamaged and damaged are reviewed and presented. A new formulation using RF applied to the damaged rod dynamic stiffness matrix was developed. This allows obtaining a close-form analytical expressions of crack depth estimation ($\alpha(\omega)$)

and crack position estimation ($L_1(\omega)$). It is based on SEM formulation and measured FRF relative change (Λ_m) including model parameter as RV and RF. The RF is expanded in a spectral decomposition known as the Karhunen-Loève expansion. Since some parameters cannot be assumed with a Gaussian marginal, for example, Young's modulus and KL expansion obeys a Gaussian distribution, a non-Gaussian translation random field is used based on memoryless nonlinear transformations. All stochastic models are solved using Monte Carlo simulation. Three different average treatment are proposed to calculate crack depth. Considering that the main interest is to obtain a single value for α and L_1, these formulations were modified by integrating the measured FRF relative change over the frequency band. One of the main advantage of the proposed spectral approach is that the analytical formulations are frequency independent. Therefore, unlike conventional finite element based approaches, there is no theoretical limitation on higher frequency ranges. However the frequency ranges can affect the longitudinal wave propagation as demonstrated in [3]. Therefore, the applicability of this work is restricted to rod in specifics frequency ranges.

All simulated examples were made using a two nodes rod spectral element in a free-free boundary condition. A sensitivity analysis of FRF relative change (Λ) relate with crack depth (α) and crack position (L_1) was performed. Crack depth analytical expression was verified and the percentage errors between nominal and calculated crack depth where lower then 10 %, using the first term of eq. 47. Including this analysis showing the influence of the polynomial degree in crack flexibility was also presented.

The formulation using parameters as RF and RV applied to the damaged and undamaged rod spectral element were verified by the mean and standard deviation of receptance FRFs with different COVs compared with deterministic receptance FRF. Results show that as the frequency and COV increase the stochastic responses increase damping behaviour. It agrees with [67] and can be explained by the average process which flattens curve peaks as the COV values increases, and at lower frequencies the standard deviation is biased by the

mean. Crack depth estimation using RV for a frequency band was evaluated for three statistical approaches to obtain Λ_m. For $\eta = 0.01$ and ($COV = 1\%$), all approaches present good approximation between calculated and nominal crack depth. As the COV's increases α_C obtained by all approaches show high dispersion around the value of α_{no} with $\Lambda_m^{(1)}$ showing the lowest dispersion. For $\eta = 0.05$ the α_C converges to α_{no} much better, but still keeping a moderate dispersion around the α_{no} at high COV's. This results agrees with [68, 69] and comes from the great influence of damping in the stochastic system the behaviour. A single crack depth value based on the stochastic response obtained from RV and RF models is calculated. Calculated crack depth and crack depth error obtained with approaches $\bar{\Lambda}_m^{(1)}$, $\bar{\Lambda}_m^{(2)}$ and $\bar{\Lambda}_m^{(3)}$ show that calculated crack depth using the approach $\bar{\Lambda}_3$ with RV model presents a good performance. The α_C using the approaches $\bar{\Lambda}_1$ and $\bar{\Lambda}_2$ with RF model present some conflicting results as the damping factor increases, which requires more investigation. Finally, random field (RF) model reveals to be unable to find out a reasonable result for α_C, independently of the approach used to calculate de FRF relative change. By locating the damage, similar procedure was adopted. A analytical expression was developed and the damage detection ia based in relative change. In all cases independently of COV and damping factor the method was able to detect the damage with acceptable errors.

Appendix A. Undamaged rod matrix elements

Appendix A.1. Stochastic

$$Ko_{11} = -\frac{e^{2ikL}k^2\left(2e^{2ikL}ik\mathrm{wj}\cos(\mathrm{wjxe})-2ik\mathrm{wj}\cos(\mathrm{wj}(L+\mathrm{xe}))+\left(4k^2-\left(1+e^{2ikL}\right)\mathrm{wj}^2\right)\sin(\mathrm{wjxe})+2\left(\mathrm{wj}^2-2k^2\right)\sin(\mathrm{wj}(L+\mathrm{xe}))\right)}{(-1+e^{2ikL})^2(\mathrm{wj}^3-4k^2\mathrm{wj})}$$

$$Ko_{12} = -\frac{k^2\left(e^{2ikL}\left(2ik\mathrm{wj}\cos(\mathrm{wj}(L+\mathrm{xe}))+\left(4k^2-\mathrm{wj}^2\right)\sin(\mathrm{wjxe})+2\left(\mathrm{wj}^2-2k^2\right)\sin(\mathrm{wj}(L+\mathrm{xe}))\right)-\mathrm{wj}(2ik\cos(\mathrm{wjxe})+\mathrm{wj}\sin(\mathrm{wjxe}))\right)}{(-1+e^{2ikL})^2(\mathrm{wj}^3-4k^2\mathrm{wj})}$$

$$Ko_{21} = Ko_{12}$$

$$Ko_{22} - \frac{e^{2ikL}k^2\left(-2ik\mathrm{wj}\cos(\mathrm{wjxe})+2e^{2ikL}ik\mathrm{wj}\cos(\mathrm{wj}(L+\mathrm{xe}))+2\left(2k^2-\mathrm{wj}^2\right)\sin(\mathrm{wjxe})-\left(4k^2-\left(1+e^{2ikL}\right)\mathrm{wj}^2\right)\sin(\mathrm{wj}(L+\mathrm{xe}))\right)}{(-1+e^{2ikL})^2(\mathrm{wj}^3-4k^2\mathrm{wj})} \tag{A.1}$$

$$Mo_{11} = \frac{e^{2ikL}\left(4\sin(\mathrm{wj}(L+\mathrm{xe}))k^2+2e^{2ikL}i\mathrm{wj}\cos(\mathrm{wjxe})k-2i\mathrm{wj}\cos(\mathrm{wj}(L+\mathrm{xe}))k-\left(4k^2+\left(-1+e^{2ikL}\right)\mathrm{wj}^2\right)\sin(\mathrm{wjxe})\right)}{(-1+e^{2ikL})^2(\mathrm{wj}^3-4k^2\mathrm{wj})}$$

$$Mo_{12} = \frac{e^{2ikL}\left(4\sin(\mathrm{wj}(L+\mathrm{xe}))k^2+2i\mathrm{wj}\cos(\mathrm{wj}(L+\mathrm{xe}))k+\left(\mathrm{wj}^2-4k^2\right)\sin(\mathrm{wjxe})\right)-\mathrm{wj}(2ik\cos(\mathrm{wjxe})+\mathrm{wj}\sin(\mathrm{wjxe}))}{(-1+e^{2ikL})^2(\mathrm{wj}^3-4k^2\mathrm{wj})}$$

$$Mo_{21} = Mo_{12}$$

$$Mo_{22} = \frac{e^{4ikL}\mathrm{wj}(2ik\cos(\mathrm{wj}(L+\mathrm{xe}))+\mathrm{wj}\sin(\mathrm{wj}(L+\mathrm{xe})))-e^{2ikL}\left(4\sin(\mathrm{wjxe})k^2+2i\mathrm{wj}\cos(\mathrm{wjxe})k+\left(\mathrm{wj}^2-4k^2\right)\sin(\mathrm{wj}(L+\mathrm{xe}))\right)}{(-1+e^{2ikL})^2(\mathrm{wj}^3-4k^2\mathrm{wj})} \tag{A.2}$$

$$Ke_{11} = -\frac{e^{2ikL}k^2\left(\left(\left(1+e^{2ikL}\right)\mathrm{wj}^2-4k^2\right)\cos(\mathrm{wjxe})+\left(4k^2-2\mathrm{wj}^2\right)\cos(\mathrm{wj}(L+\mathrm{xe}))+2ik\mathrm{wj}\left(e^{2ikL}\sin(\mathrm{wjxe})-\sin(\mathrm{wj}(L+\mathrm{xe}))\right)\right)}{(-1+e^{2ikL})^2(\mathrm{wj}^3-4k^2\mathrm{wj})}$$

$$Ke_{12} = -\frac{k^2\left(\mathrm{wj}(\mathrm{wj}\cos(\mathrm{wjxe})-2ik\sin(\mathrm{wjxe}))+e^{2ikL}\left(\left(\mathrm{wj}^2-4k^2\right)\cos(\mathrm{wjxe})+\left(4k^2-2\mathrm{wj}^2\right)\cos(\mathrm{wj}(L+\mathrm{xe}))+2ik\mathrm{wj}\sin(\mathrm{wj}(L+\mathrm{xe}))\right)\right)}{(-1+e^{2ikL})^2(\mathrm{wj}^3-4k^2\mathrm{wj})}$$

$$Ke_{21} = Ke_{12}$$

$$Ke_{22} = -\frac{e^{2ikL}k^2\left(2\left(\mathrm{wj}^2-2k^2\right)\cos(\mathrm{wjxe})+\left(4k^2-\left(1+e^{2ikL}\right)\mathrm{wj}^2\right)\cos(\mathrm{wj}(L+\mathrm{xe}))-2ik\mathrm{wj}\left(\sin(\mathrm{wjxe})-e^{2ikL}\sin(\mathrm{wj}(L+\mathrm{xe}))\right)\right)}{(-1+e^{2ikL})^2(\mathrm{wj}^3-4k^2\mathrm{wj})} \tag{A.3}$$

$$Me_{11} = \frac{e^{2ikL}\left(\left(4k^2+\left(-1+e^{2ikL}\right)\mathrm{wj}^2\right)\cos(\mathrm{wjxe})+2ik\left(2ik\cos(\mathrm{wj}(L+\mathrm{xe}))+e^{2ikL}\mathrm{wj}\sin(\mathrm{wjxe})-\mathrm{wj}\sin(\mathrm{wj}(L+\mathrm{xe}))\right)\right)}{(-1+e^{2ikL})^2(\mathrm{wj}^3-4k^2\mathrm{wj})}$$

$$Me_{12} = \frac{\mathrm{wj}(\mathrm{wj}\cos(\mathrm{wjxe})-2ik\sin(\mathrm{wjxe}))+e^{2ikL}\left(-4\cos(\mathrm{wj}(L+\mathrm{xe}))k^2+2i\mathrm{wj}\sin(\mathrm{wj}(L+\mathrm{xe}))k+\left(4k^2-\mathrm{wj}^2\right)\cos(\mathrm{wjxe})\right)}{(-1+e^{2ikL})^2(\mathrm{wj}^3-4k^2\mathrm{wj})}$$

$$Me_{21} = Me_{12}$$

$$Me_{22} = \frac{e^{2ikL}\left(4\cos(\mathrm{wjxe})k^2-2i\mathrm{wj}\left(\sin(\mathrm{wjxe})-e^{2ikL}\sin(\mathrm{wj}(L+\mathrm{xe}))\right)k+\left(-4k^2-e^{2ikL}\mathrm{wj}^2+\mathrm{wj}^2\right)\cos(\mathrm{wj}(L+\mathrm{xe}))\right)}{(-1+e^{2ikL})^2(\mathrm{wj}^3-4k^2\mathrm{wj})} \tag{A.4}$$

Appendix B. Damaged rod matrix elements

Appendix B.1. Deterministic

$$\begin{aligned}
K_{0d_{11}} &= EAk\Big\{\Big[4\left(k\left(\Theta\left(k^2L_1\Theta-1\right)+2L\right)+\sin(2kL)\right)+k\Theta\Big(4\left(k^2L_1\Theta-1\right)\cos(2k(L-L_1)) \\
&\quad + k(\Theta(\sin(2k(L-2L_1))-\sin(2kL)-2\sin(2kL_1))+8L_1\sin(2k(L-L_1)))+4\cos(2kL) \\
&\quad + 4\cos(2kL_1)\Big)\Big]\Big/\Big[4(k\Theta(\cos(k(L-2L_1))+\cos(kL))+2\sin(kL))^2\Big]\Big\} \\
K_{0d_{12}} &= EAk\Big\{\frac{\left(k^2\Theta(L-2L_1)\sin(k(L-2L_1))+\left(k^2L\Theta-2\right)\sin(kL)-2kL\cos(kL)\right)}{(k\Theta(\cos(k(L-2L_1))+\cos(kL))+2\sin(kL))^2}\Big\} \\
K_{0d_{21}} &= K_{0d_{12}} \\
K_{0d_{22}} &= EAk\Big\{\Big[4\left(k^3\Theta^2(L-L_1)+2kL+\sin(2kL)-k\Theta\right)+k\Theta Bigl(4\cos(2kL_1)\left(k^2\Theta(L-L_1)-1\right) \\
&\quad - k\Theta(\sin(2k(L-2L_1))+2\sin(2k(L-L_1))+\sin(2kL))+8k(L-L_1)\sin(2kL_1)+4\cos(2k(L-L_1)) \\
&\quad + 4\cos(2kL)\Big)\Big]\Big/\Big[4(k\Theta(\cos(k(L-2L_1))+\cos(kL))+2\sin(kL))^2\Big]\Big\}
\end{aligned} \tag{B.1}$$

$$\begin{aligned}
M_{0d_{11}} &= \rho A\Big\{\Big[4k\left(k^2L_1\Theta^2+\Theta+2L\right)-4\sin(2kL)+k\Theta\Big(-4\cos(2kL)+4\left(L_1\Theta k^2+1\right)\cos(2k(L-L_1)) \\
&\quad - 4\cos(2kL_1)+8kL_1\sin(2k(L-L_1))+k\Theta(\sin(2kL)-\sin(2k(L-2L_1))+2\sin(2kL_1))\Big)\Big]\Big/\Big[4k\Big(k\Theta\Big(\cos(kL) \\
&\quad + \cos(k(L-2L_1))\Big)+2\sin(kL)\Big)^2\Big]\Big\} \\
M_{0d_{12}} &= \rho A\Big\{\frac{(L-2L_1)\Theta\sin(k(L-2L_1))k^2-2L\cos(kL)k+\left(L\Theta k^2+2\right)\sin(kL)}{k(k\Theta(\cos(kL)+\cos(k(L-2L_1)))+2\sin(kL))^2}\Big\} \\
M_{0d_{21}} &= M_{0d_{12}} \\
M_{0d_{22}} &= \rho A\Big\{\Big[4k\left(k^2(L-L_1)\Theta^2+\Theta+2L\right)-4\sin(2kL)+k\Theta\Big(-4\cos(2kL)-4\cos(2k(L-L_1)) \\
&\quad + 4\left((L-L_1)\Theta k^2+1\right)\cos(2kL_1)+k\Theta(\sin(2kL)+\sin(2k(L-2L_1))+2\sin(2k(L-L_1))) \\
&\quad + 8k(L-L_1)\sin(2kL_1)\Big)\Big]\Big/\Big[4k(k\Theta(\cos(kL)+\cos(k(L-2L_1)))+2\sin(kL))^2\Big]\Big\}
\end{aligned} \tag{B.2}$$

Appendix B.2. Stochastic

$$SkLo_{11} = -\frac{k^2\left(-2ik\cos(\mathrm{wjxe})+2e^{-2ikL_1}ik\cos(\mathrm{wj}(L_1+\mathrm{xe}))+\mathrm{wj}\sin(\mathrm{wjxe})-e^{-2ikL_1}\mathrm{wj}\sin(\mathrm{wj}(L_1+\mathrm{xe}))\right)}{4k^2-\mathrm{wj}^2}$$

$$SkLo_{12} = \frac{e^{-ikL_1}k^2(\sin(\mathrm{wj}(L_1+\mathrm{xe}))-\sin(\mathrm{wjxe}))}{\mathrm{wj}}$$

$$SkLo_{21} = SkLo_{12}; \qquad SkLo_{22} = -\frac{k^2\left(2e^{-2ikL_1}ik\cos(\mathrm{wjxe})-2ik\cos(\mathrm{wj}(L_1+\mathrm{xe}))+e^{-2ikL_1}\mathrm{wj}\sin(\mathrm{wjxe})-\mathrm{wj}\sin(\mathrm{wj}(L_1+\mathrm{xe}))\right)}{4k^2-\mathrm{wj}^2}$$

$$SmLo_{11} = \frac{-2ik\cos(\mathrm{wjxe})+\mathrm{wj}\sin(\mathrm{wjxe})+e^{-2ikL_1}(2ik\cos(\mathrm{wj}(L_1+\mathrm{xe}))-\mathrm{wj}\sin(\mathrm{wj}(L_1+\mathrm{xe})))}{4k^2-\mathrm{wj}^2}$$

$$SmLo_{12} = \frac{e^{-ikL_1}(\sin(\mathrm{wj}(L_1+\mathrm{xe}))-\sin(\mathrm{wjxe}))}{\mathrm{wj}}$$

$$SmLo_{21} = SmLo_{12}; \qquad SmLo_{22} = \frac{-2ik\cos(\mathrm{wj}(L_1+\mathrm{xe}))+e^{-2ikL_1}(2ik\cos(\mathrm{wjxe})+\mathrm{wj}\sin(\mathrm{wjxe}))-\mathrm{wj}\sin(\mathrm{wj}(L_1+\mathrm{xe}))}{4k^2-\mathrm{wj}^2}$$

$$SkRo_{11} = -\frac{k^2\left(e^{-2ikL_1}(\mathrm{wj}\sin(\mathrm{wjxe})-2ik\cos(\mathrm{wjxe}))+e^{-2ikL}(2ik\cos(\mathrm{wj}(L-L_1+\mathrm{xe}))-\mathrm{wj}\sin(\mathrm{wj}(L-L_1+\mathrm{xe})))\right)}{4k^2-\mathrm{wj}^2}$$

$$SkRo_{12} = \frac{e^{-ikL}k^2(\sin(\mathrm{wj}(L-L_1+\mathrm{xe}))-\sin(\mathrm{wjxe}))}{\mathrm{wj}}$$

$$SkRo_{21} = SkRo_{12}; \qquad SkRo_{22} = \frac{k^2\left(2ik\cos(\mathrm{wj}(L-L_1+\mathrm{xe}))-ie^{2ik(L_1-L)}(2k\cos(\mathrm{wjxe})-i\mathrm{wj}\sin(\mathrm{wjxe}))+\mathrm{wj}\sin(\mathrm{wj}(L-L_1+\mathrm{xe}))\right)}{4k^2-\mathrm{wj}^2}$$

$$SmRo_{11} = \frac{e^{-2ikL_1}(\mathrm{wj}\sin(\mathrm{wjxe})-2ik\cos(\mathrm{wjxe}))+e^{-2ikL}(2ik\cos(\mathrm{wj}(L-L_1+\mathrm{xe}))-\mathrm{wj}\sin(\mathrm{wj}(L-L_1+\mathrm{xe})))}{4k^2-\mathrm{wj}^2}$$

$$SmRo_{12} = \frac{e^{-ikL}(\sin(\mathrm{wj}(L-L_1+\mathrm{xe}))-\sin(\mathrm{wjxe}))}{\mathrm{wj}}$$

$$SmRo_{21} = SmRo_{12}; \qquad SmRo_{22} = \frac{-2ik\cos(\mathrm{wj}(L-L_1+\mathrm{xe}))+e^{2ik(L_1-L)}(2ik\cos(\mathrm{wjxe})+\mathrm{wj}\sin(\mathrm{wjxe}))-\mathrm{wj}\sin(\mathrm{wj}(L-L_1+\mathrm{xe}))}{4k^2-\mathrm{wj}^2}$$

$$SkLe_{11} = -\frac{k^2\left(-\mathrm{wj}\cos(\mathrm{wjxe})+e^{-2ikL_1}\mathrm{wj}\cos(\mathrm{wj}(L_1+\mathrm{xe}))-2ik\sin(\mathrm{wjxe})+2e^{-2ikL_1}ik\sin(\mathrm{wj}(L_1+\mathrm{xe}))\right)}{4k^2-\mathrm{wj}^2}$$

$$SkLe_{12} = \frac{e^{-ikL_1}k^2(\cos(\mathrm{wjxe})-\cos(\mathrm{wj}(L_1+\mathrm{xe})))}{\mathrm{wj}}$$

$$SkLe_{21} = SkLe_{12}; \qquad SkLe_{22} = -\frac{k^2\left(-e^{-2ikL_1}\mathrm{wj}\cos(\mathrm{wjxe})+\mathrm{wj}\cos(\mathrm{wj}(L_1+\mathrm{xe}))+2ik\left(e^{-2ikL_1}\sin(\mathrm{wjxe})-\sin(\mathrm{wj}(L_1+\mathrm{xe}))\right)\right)}{4k^2-\mathrm{wj}^2}$$

$$SmLe_{11} = \frac{-\mathrm{wj}\cos(\mathrm{wjxe})-2ik\sin(\mathrm{wjxe})+e^{-2ikL_1}(\mathrm{wj}\cos(\mathrm{wj}(L_1+\mathrm{xe}))+2ik\sin(\mathrm{wj}(L_1+\mathrm{xe})))}{4k^2-\mathrm{wj}^2}$$

$$SmLe_{12} = +\frac{e^{-ikL_1}(\cos(\mathrm{wjxe})-\cos(\mathrm{wj}(L_1+\mathrm{xe})))}{\mathrm{wj}}$$

$$SMe^1_{21} = SMe^1_{12}; \qquad SmLe_{22} = \frac{\mathrm{wj}\cos(\mathrm{wj}(L_1+\mathrm{xe}))+e^{-2ikL_1}(2ik\sin(\mathrm{wjxe})-\mathrm{wj}\cos(\mathrm{wjxe}))-2ik\sin(\mathrm{wj}(L_1+\mathrm{xe}))}{4k^2-\mathrm{wj}^2}$$

$$SkRe_{11} = -\frac{k^2\left(e^{-2ikL}(\mathrm{wj}\cos(\mathrm{wj}(L-L_1+\mathrm{xe}))+2ik\sin(\mathrm{wj}(L-L_1+\mathrm{xe})))-e^{-2ikL_1}(\mathrm{wj}\cos(\mathrm{wjxe})+2ik\sin(\mathrm{wjxe}))\right)}{4k^2-\mathrm{wj}^2}$$

$$SkRe_{12} = \frac{e^{-ikL}k^2(\cos(\mathrm{wjxe})-\cos(\mathrm{wj}(L-L_1+\mathrm{xe})))}{\mathrm{wj}}$$

$$SkRe_{21} = SkRe_{12}; \qquad SkRe_{22} = \frac{k^2\left(-\mathrm{wj}\cos(\mathrm{wj}(L-L_1+\mathrm{xe}))+e^{2ik(L_1-L)}(\mathrm{wj}\cos(\mathrm{wjxe})-2ik\sin(\mathrm{wjxe}))+2ik\sin(\mathrm{wj}(L-L_1+\mathrm{xe}))\right)}{4k^2-\mathrm{wj}^2}$$

$$SmRe_{11} = \frac{e^{-2ikL}(\mathrm{wj}\cos(\mathrm{wj}(L-L_1+\mathrm{xe}))+2ik\sin(\mathrm{wj}(L-L_1+\mathrm{xe})))-e^{-2ikL_1}(\mathrm{wj}\cos(\mathrm{wjxe})+2ik\sin(\mathrm{wjxe}))}{4k^2-\mathrm{wj}^2}$$

$$SmRe_{12} = \frac{e^{-ikL}(\cos(\mathrm{wjxe})-\cos(\mathrm{wj}(L-L_1+\mathrm{xe})))}{\mathrm{wj}}$$

$$SmRe_{21} = SmRe_{12}; \qquad SmRe_{22} = \frac{\mathrm{wj}\cos(\mathrm{wj}(L-L_1+\mathrm{xe}))+e^{2ik(L_1-L)}(2ik\sin(\mathrm{wjxe})-\mathrm{wj}\cos(\mathrm{wjxe}))-2ik\sin(\mathrm{wj}(L-L_1+\mathrm{xe}))}{4k^2-\mathrm{wj}^2}$$

References

[1] S. W. Doebling, C. R. Farrar, M. Prime, A review of vibration-based damage identification methods, Tech. rep., Engineering Analysis Group Los Alamos National Laboratory (1998).

[2] D. Montalvo, N. Maia, A. Ribeiro, A review of vibration-based structural health monitoring with special emphasis on composite materials, The Shock and Vibration Digest 38 (2006) 295 – 324.

[3] M. Krawczuk, J. Grabowska, M. Palacz, Longitudinal wave propagation. Part I - Comparison of rod theories, Journal of Sound and Vibration 295 (2006) 461–478. doi:10.1016/j.jsv.2005.12.048.

[4] M. Krawczuk, Application of spectral beam finite element with a crack and iterative search technique for damage detection, Finite Elements in Analysis and Design 80 (2002) 1809–1816. doi:10.1016/S0168-874X(01)00084-1.

[5] W. M. Ostachowicz, Damage detection of structures using spectral finite element method, Computers & Structures 86 (2008) 454–462. doi:10.1016/j.compstruc.2007.02.004.

[6] Z. Su, L. Ye, Identification of Damage Using Lamb Waves, Springer, 2009.

[7] E. Santos, J. Arruda, J. D. Santos, Modeling of coupled structural systems by an energy spectral element method, Journal of Sound and Vibration 36 (2008) 1 – 24.

[8] J. F. Doyle, Wave propagation in structures : spectral analysis using fast discrete Fourier transforms, 2nd Edition, Mechanical engineering, Springer-Verlag New York, Inc., New York, 1997.

[9] U. Lee, Spectral Element Method in Structural Dynamics, BInha University Press, 2004.

[10] M. Paz, Structural Dynamics: Theory and Computation, 2nd Edition, Van Nostrand, Reinhold, 1980.

[11] J. R. Banerjee, F. W. Williams, Exact bernoulli-euler dynamic stiffness matrix for a range of tapered beams, International Journal for Numerical Methods in Engineering 21 (12) (1985) 2289–2302.

[12] J. R. Banerjee, Coupled bending torsional dynamic stiffness matrix for beam elements, International Journal for Numerical Methods in Engineering 28 (6) (1989) 1283–1298.

[13] J. R. Banerjee, F. W. Williams, Coupled bending-torsional dynamic stiffness matrix for timoshenko beam elements, Computer and Structures 42 (3) (1992) 301–310.

[14] J. R. Banerjee, S. A. Fisher, Coupled bending torsional dynamic stiffness matrix for axially loaded beam elements, International Journal for Numerical Methods in Engineering 33 (4) (1992) 739–751.

[15] N. J. Ferguson, W. D. Pilkey, Literature review of variants of dynamic stiffness method, Part 1: The dynamic element method, The Shock and Vibration Digest 25 (2) (1993) 3–12.

[16] N. J. Ferguson, W. D. Pilkey, Literature review of variants of dynamic stiffness method, Part 2: Frequency-dependent matrix and other, The Shock and Vibration Digest 25 (4) (1993) 3–10.

[17] J. R. Banerjee, F. W. Williams, Free-vibration of composite beams - an exact method using symbolic computation, Journal of Aircraft 32 (3) (1995) 636–642.

[18] C. S. Manohar, S. Adhikari, Dynamic stiffness of randomly parametered beams, Probabilistic Engineering Mechanics 13 (1) (1998) 39–51.

[19] J. R. Banerjee, Dynamic stiffness formulation for structural elements: A general approach, Computer and Structures 63 (1) (1997) 101–103.

[20] S. Adhikari, C. S. Manohar, Transient dynamics of stochastically parametered beams, ASCE Journal of Engineering Mechanics 126 (11) (2000) 1131–1140.

[21] J. F. Doyle, Wave Propagation in Structures, Springer Verlag, New York, 1989.

[22] S. Gopalakrishnan, A. Chakraborty, D. R. Mahapatra, Spectral Finite Element Method, Springer Verlag, New York, 2007.

[23] S. M. Hashemi, M. J. Richard, G. Dhatt, A new Dynamic Finite Element (DFE) formulation for lateral free vibrations of Euler-Bernoulli spinning beams using trigonometric shape functions, Journal of Sound and Vibration 220 (4) (1999) 601–624.

[24] S. M. Hashemi, M. J. Richard, Free vibrational analysis of axially loaded bending-torsion coupled beams: a dynamic finite element, Computer and Structures 77 (6) (2000) 711–724.

[25] M. P. M. Krawczuk, Analysis of longitudinal wave propagation in a cracked rod by the spectral element method, Computers & Structures 80 (24) (2002) 1809–1816. doi:10.1016/S0045-7949(02)00219-5.

[26] M.V.V.S. Murthy and S. Gopalakrishnan and P.S. Nair, Signal wrap around free spectral finite element formulation for multiply connected 1d wave guides, Journal of Aerospace Sciences & Technologies 63 (2011) 72–88.

[27] S. Adhikari, M. Friswell, Distributed parameter model updating using the Karhunen-Loève expansion, Mechanical Systems and Signal Processing 24 (2010) 326–339.

[28] V. Ajith, S. Gopalakrishnan, Spectral element approach to wave propagation in uncertain beam structures, Journal of Mechanics of Material and Structures 5(4) (2010) 637–659.

[29] A. T. Fabro, T. G. Ritto, R. Sampaio, J. R. F. Arruda, Stochastic analysis of a cracked rod modeled via the spectral element method, Mechanics Research Communications 37 (2010) 326–331. doi:10.1016/j.mechrescom.2010.03.005.

[30] C. Ng, M. Veidt, H. Lam, Probabilistic damage characterisation in beams using guided waves, Procedia Engineering 14 (2011) 490 – 497.

[31] J. C. B. D. E. B. Flynn, M.D. Todd, P. Wilcox, Enhanced detection through low-order stochastic modeling for guided-wave structural health monitoring, Structural Health Monitoring.

[32] M. R. Machado, J. M. C. D. Santos, Reliability analysis of damaged beam spectral element with parameter uncertainties, Shock and Vibration 2015 (2015) 12 pages. doi:10.1155/2015/574846.

[33] C. R. Farrar, K. Worden, An introduction to structural health monitoring, Philosophical Transactions of the Royal Society 365 (2007) 303 – 315.

[34] S. W. Doebling, C. R. Farrar, M. Prime, D. W. Shevitz, Damage identification and health monitoring of structural and mechanical systems from changes in their vibration characteristics- a literature review, Tech. rep., Los Alamos National Laboratory -University of California (1996).

[35] R. C. Aster, C. H. Thurber, Parameter estimation and inverse problems, Academic Press publications, 2012.

[36] M. I. Friswell, Damage identification using inverse methods, Philosophical Transactions of the Royal Society 2007 (2007) 393 – 410.

[37] J. E. Mottershead, M. Friswell, Model updating in strucutral dynamics: A survey, Journal of Sound and Vibration 167(2) (1993) 347– 375.

[38] C. Fritzen, D. Jennewein, Damage detection based on model updating methods, Mechanical Systems and Signal Processing 12(1) (1998) 163 – 186.

[39] M. I. Friswell, J. E. Mottershead, Finite element model updating in structural dynamics, Kluwer Academic Publishers, 1995.

[40] A. Morassi, F. Vestroni, Dynamic methods for damage detection in strucutres, Springer New York, 2008.

[41] J. M. C. DosSantos, D. C. Zimmerman, Structural damage detection using minimum rank update theory and parameter estimation, in: Proceedings of the AIAA/ASME/AHS Adaptive Structures Forum, 1996.

[42] O. C. Zienkiewicz, R.L.Taylor, The Finite Element Method, Butterworth-Heinemann, 2000.

[43] N. M. Maia, M. Julio, Theoretical and Experimental Modal Analysis, Research Studies Pre, 1997.

[44] Y. Xu, J. Zhang, J. Li, X. Wang, Stochastic damage detection method for building structures with parametric uncertainties, Journal of Sound and Vibration 330 (2011) 4725 – 4737.

[45] O. ArdaVanli, S. Jung, Statistical updating of finite element model with lamb wave sensing data for damage detection problems, Mechanical Systems and Signal Processing.

[46] H. H. Khodaparast, J. Mottershead, Efficient methods in stochastic model updating, in: Proceedings of ISMA, 2008.

[47] A. Papoulis, S. U. Pillai, Probability, random variables and stochastic processes., McGraw-Hill, Boston, 2002.

[48] I. M. Sobol', A primer for the Monte Carlo method, CRC Press, 1994.

[49] D. Xiu, Numerical Methods for Computations-A Spectral method approcah, Princeton University Press, 2010.

[50] R. Ghanem, P. Spanos, Stochastic Finite Elements - A Spectral Approach, Springer, 1991.

[51] M. Grigoriu, Simulation of Stationary Non-Gaussian Translation Processes, Journal of Engineering Mechanics 124 (1998) 121–126. doi:10.1061/(ASCE)0733-9399(1998)124:2(121).

[52] F. Poirion, C. Soize, Monte carlo construction of karhunen-loeve expansion for non-gaussian random fields, in: Proceedings of the 13th ASCE Engineering Mechanics Division Conference, 1999.

[53] R. Vio, P. Andreani, W. Wamsteker, Nmerical simularin of non-gaussian random fields with prescribed correlation structure, Tech. rep., ESA IUE Obsevatory and Max-Planck Institut fur Extraterrestrische Physik (2001).

[54] P. F. Puig, B., C. Soize, Non-gaussian simulation using hermite polynomial expansion: convergences and algorithms, Probabilistic Engineering Mechanics 17(3) (2002) 253Dc264. doi:10.1016/S0266-8920(02)00010-3.

[55] S.Sakamoto, R. Ghanem, Simulation of multi-dimensional non-Gaussian non-stationary random fields., Probabilistic Engineering Mechanics 17 (2002) 167–176.

[56] G. L. M. Schevenels, G. Degrande, Application of the stochastic finite element method for gaussian and non-gaussian systems, in: Proceedings of International Conference on Noise and Vibration Engineering, 2004.

[57] H. H. W. Phoon K. K., S. T. Quek, Simulation of strongly non-gaussian processes using karhunen-loeve expansion, Structural Safety 20(2) (2005) 1881198. doi:10.1016/j.probengmech.2005.05.007.

[58] G. Weinberg, L.Gunn, Simulation of statistical distributions using the memoryless nonlinear transformation, Tech. rep., DSTO Defence Science and Technology Organisation-Australia Government (2011).

[59] M. Hazewinkel, Encyclopaedia of Mathematics:Fibonacci Method-H, Springer Science & Business Media., 1989.

[60] D. Xiu, G. E. Karniadakis, The Wiener-Askey polynomial chaos for stochastic differential equations, Tech. rep., Brown University,Division of Applied Mathematics,182 George Street,Providence,RI (2003).

[61] M. Krawczuk, J. Grabowska, M. Palacz, Longitudinal wave propagation. Part II-Analysis of crack influence, Journal of Sound and Vibration 295 (2006) 479–490. doi:10.1016/j.jsv.2005.12.049.

[62] H. Tada, P. Paris, G. R. Irwin, Stress Analysis of Cracks Handbook, Del Research Corporation, 1973.

[63] E. E. Gdoutos, Fracture Mechanics: an Introduction, Ed. Kluwer Academic Publishers, 1993.

[64] J.-J. Sinou, Numerical investigations of a robust identification of crack location and size in beams using only changes in ratio pulsations of the cracked beams, Structural Engineering Mechanics 25(6) (2007) 691–716.

[65] Y. Narkis, Identification of crack location in vibrating simply supported beams, Journal of Sound and Vibration 172(4) (1994) 549 – 558.

[66] J.-J. Sinou, A Review of Damage Detection and Health Monitoring of Mechanical Systems from Changes in the Measurement of Linear and Non-linear Vibrations, Tech. rep., Laboratoire de Tribologie et Dynamique des Systemes UMR-CNRS 5513 Ecole Centrale de Lyon (2013).

[67] S. Adhikari, Doubly spectral stochastic finite-element method for linear structural dynamics, American Society of Civil Engineers 1 (2011) 264–276.

[68] R. Pavlovic, P. Kozic, P. Rajkovic, Influence of randomly varying damping coefficient on the dynamic stability of continuous systems, European Journal of Mechanics A/Solids 24 (2005) 8187.

[69] S. Adhikari, Structural Dynamic Analysis with Generalized Damping Models, Wiley, 2013.